Inter-Comparison of the ELDAS models Using the Rhone-AGGregation Experimental design

Aaron Boone, Florence Habets, Joel Noilhan, Bart Van den Hurk, Martin Lange, Jose Parodi, Bodo Ritter and E. Rodriguez

October, 2003

Centre National de Recherches Météorologiques,Météo-France

42, avenue G. Coriolis, 31057 TOULOUSE Cedex France

Affiliations

Aaron Boone[a,b], Florence Habets[a], Joel Noilhan[a],

Bart Van den Hurk[c], Martin Lange[d], Jose Parodi[e],

Bodo Ritter[d] and E. Rodriguez[e]

a CNRM-Météo-France, Toulouse, France

b Centres d'Etudes Spatiales de la BIOsphére, Toulouse, France

c KNMI (Dutch MetOffice), De Bilt, The Netherlands

d Deutscher Wetterdienst (German Weather Service), Offenbach, Germany

e I.N.M., Numerical Weather Prediction Dept., Madrid, Spain

Executive Summary

This report presents a summary of an intercomparison and evaluation of the simulations by the land surface schemes (LSSs) from the ELDAS (European Land Data Assimilation System) project using the Rhône-Aggregation (Rhône-AGG: Boone et al. 2003) experimental setup. The Rhône-AGG is an initiative within the Global Energy and Water Cycle Experiment (GEWEX) Global Land-Atmosphere System Study (GLASS: Polcher, 2001), and it is an intermediate step leading up to the Global Soil Wetness Project (Dirmeyer et al. 1999) Phase 2. The simulations of the regional hydrological cycle by the ELDAS LSSs are evaluated and also compared with the Rhône aggregation participant LSSs. In all, the results from 25 three-year simulations are examined. The LSSs were driven in off-line mode by atmospheric forcing from the SAFRAN system of Météo-France, and a full set of vegetation and soil parameters were provided by CNRM for the Rhône basin in south-eastern France. The results are also evaluated using the observed snow depth at 24 sites and the river discharge for 112 basins.

TABLE OF CONTENTS

Chapter 1. Introduction 4

Chapter 2. Database and Experiment 7
1. Forcing and Parameter Data 7
2. Hydrological Model 10
3. LSS interface 11
4. Observations for LSS Evaluation 12

Chapter 3. Results 13
1. Setup 13
2. Simulations 15
   a. Energy and Water Balance 16
      1) Soil Moisture 23
   b. Snow Simulation 28
   c. River Discharge 34
      1) Rhône-AGG special basins 34
      2) River Discharge: All basins 42

Chapter 4. Summary 47

Appendix A. ALMA Variable Names 49

Appendix B. Statistical Measures 50

References 51

CHAPTER 1

INTRODUCTION

The regional water cycle has become an increasingly studied phenomena in recent years owing to a variety of factors, such as dwindling fresh water resources relative to the ever-growing human population, the predicted adverse impacts of a theorized global warming, changes in water use because of anthropogenic effects (such as dams and irrigation), and changes in precipitation patterns due to natural climatic variability. One method used by the scientific community to improve the understanding of this complex system is the utilization of atmospheric and hydrological models. Significant improvements have been achieved in recent years, but there is still a lack of understanding of some of the basic mechanisms at work and how to accurately model them.

Atmospheric modelers attempt to improve the simulation of the hydrological cycle through the physical parameterizations related to precipitation. Hydrological modelers generally use relatively simple empirically-based production functions as upper boundary conditions, while giving more detailed attention to subterranean water movement and river routing. The link between these models is the Land-Surface-Scheme (LSS) which has the main functions of partitioning incoming atmospheric energy into fluxes of radiation, heat, mass and momentum, and dividing the incoming precipitation into storage, runoff and evaporative components. The LSS is therefore a key component of the simulation of the hydrological cycle.

Numerous field experiments have been done over the years with the objective of improving the understanding of the link between the land-surface and the

atmosphere. Some examples of some of the most published studies are HAPEX-MOBILHY (André et al. 1986), FIFE (Sellers et al. 1988), BOREAS (Sellers et al. 1997), and Cabauw, the Netherlands (Beljaars and Bosveld 1997). These data sets have proven to be of value in terms of LSS model development, evaluation and intercomparison studies. In particular, the Project for the Intercomparison of Land-surface Parameterization Schemes (PILPS: Henderson-Sellers et al. 1993) has increased the understanding of LSS models, and it has lead to many improvements in the schemes themselves. In Phase-2 of PILPS (Henderson-Sellers et al. 1995), LSSs have been used in so-called "off-line mode" (driven using prescribed atmospheric forcing), and the resulting simulations have been compared to observed data. Atmospheric data representing a local scale or an atmospheric model grid box were used by PILPS phases 2a (Cabauw: Chen et al. 1997) and 2b (HAPEX-MOBILHY: Shao and Henderson-Sellers 1996) for a single annual cycle, and phase 2d (Schlosser et al. 2000) for a multi-year simulation. The primary results of these studies showed the importance of the model parameterizations of soil moisture, the link between soil water (stress) and transpiration, and cold-season processes, respectively.

The first attempt by PILPS to address LSS behavior at a regional scale was undertaken in PILPS-2c (Wood et al. 1998). Multi-year basin-scale LSS simulations over the southern Central Plains of the US were evaluated using a river routing model and observed daily river discharge. Subgrid runoff parameterizations were shown to be of critical importance in terms of correctly simulating river discharge for the spatial scales considered (1x1 degree grid elements). PILPS-2e (Bowling et al., 2003) is similar to Phase-2c, except that the basin is located at a relatively high latitude with a considerable coverage of lakes and wetlands (at a 1/4 x 1/4 degree spatial resolution). River flows are controlled to a large extent by lake and soil freeze-thaw and snow melt.

The GSWP (Phase 1: Dirmeyer et al. 1999) was an "off-line" LSS intercomparison study which produced 2-year global data sets of soil moisture, surface fluxes, and related hydrological quantities. This project was used as a means for testing and developing large-scale validation techniques over land, it served as a large-scale validation and quality check of the ISLSCP Initiative I (Meeson et al. 1995; Sellers et al. 1995) data sets, it undertook a global comparison of a number of LSSs, and it included a series of sensitivity studies of specific parameterizations (which lead to improvements in some models).

The most recent basin or regional scale LSS-intercomparison project is the Rhône-AGGregation experiment (Rhône-AGG: Boone et al. 2003), which is an initiative within the Global Energy and Water Cycle Experiment (GEWEX) Global Land-Atmosphere System Study (GLASS: Polcher et al. 2000). It is an intermediate step leading up to the GSWP-Phase 2, for which there will be a broader investigation of the aggregation between global scales (GSWP-1) and the river scale. This project differs from the aforementioned PILPS basin-scale studies because the very high spatial resolution observational data within the Rhône basin provides an exceptional database for model evaluation, and it makes it possible to examine the impact of scaling on LSS simulations. Because of the quality of the observational data, the European Land-Data-Assimilation System (ELDAS) project has utlized the Rhône-AGG experimental setup as an initial evaluation step. In this report, simulation results from five ELDAS LSSs are evaluated and compared to results from 13 other state-of-the-art schemes.

CHAPTER 2

DATABASE AND EXPERIMENT

The Rhône is the largest European river flowing into the Mediterranean Sea. The corresponding basin covers over 86,000 km^2 of south-eastern France (Fig. 2.1). Surface characteristics, sub-surface parameters and atmospheric forcing are mapped onto this domain under the fellowship of the GEWEX-Rhône project, which was conceived in recent years by the French research community in order to study the continental water cycle on a regional scale.

The ultimate goal of the GEWEX-Rhône project is to develop a full dynamic coupling between an atmospheric model, a LSS and a river routing model (Etchevers et al. 2001). The first phase of this project consists in coupling a LSS with a distributed hydrological model in order to improve both the estimation of evapotranspiration and the partitioning of the LSS-computed runoff between the fast (surface runoff and lateral flow) and slow (drainage or baseflow) time response components. Three distinct components comprise the corresponding modeling system (Habets et al. 1999b): an analysis system to determine the near-surface atmospheric forcing, a LSS interface and a distributed hydrological model. The coupling between the components of the system is 1-way (as shown in the schematic in Fig. 2.2), and the variables transferred between each component are indicated in the rectangles connected to arrows.

1. Forcing and Parameter Data

The domain is divided up into 1,471 8 x 8 km grid boxes. The gridded topography is shown using 500 m increments in Fig. 2.1. The atmospheric forcing is

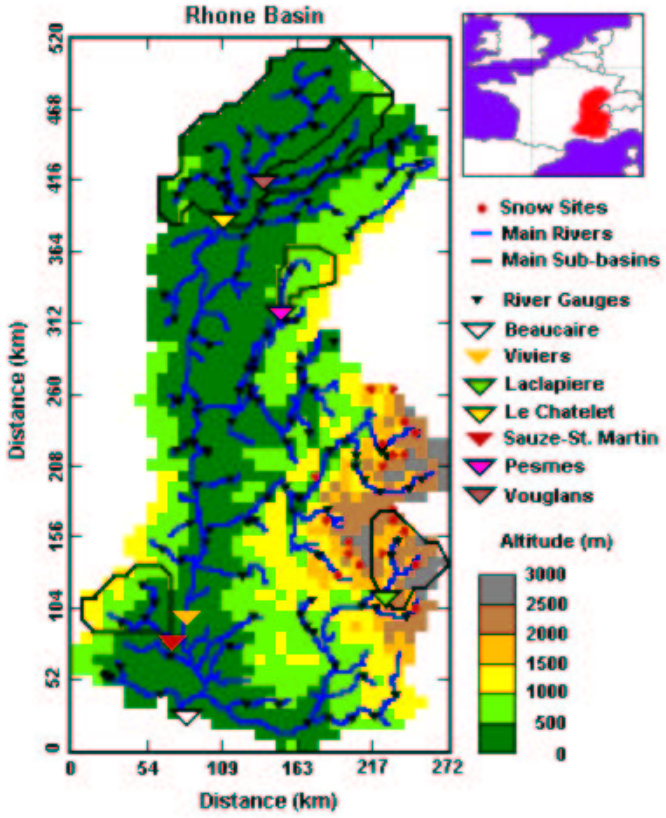

FIG. 2.1. The Rhône model domain. The gridded topography is shown at 500 m intervals. The locations of the 145 gauging stations are represented by the filled triangles and the snow observation sites are indicated by the filled red circles. The major rivers are shown in blue. The three sub-basins given special treatment in Rhône-AGG are outlined, along with two used for model calibration. The location of the basin relative to France is also shown.

calculated using the SAFRAN (Système d'Analyse Fournissant des Renseignements Atmosphériques à la Neige: Analysis System for Providing Atmospheric Information relevant to Snow) analysis system (Durand et al. 1993). The input atmospheric data consist of standard screen level observations at approximately 60 Météo-France weather network sites within the domain, ECMWF analyses and climatological data for 249 homogeneous climatic zones, and total daily precipitation data from over 1500 gauges (see Fig. 2.3).

The provided forcing variables (at a three-hour time interval) are the air temperature at 2 m, wind speed at 10 m, specific humidity at 2 m, down-welling visible solar radiation, down-welling long-wave atmospheric radiation, liquid precipitation rate, liquid water equivalent snow/solid precipitation rate, and surface pressure.

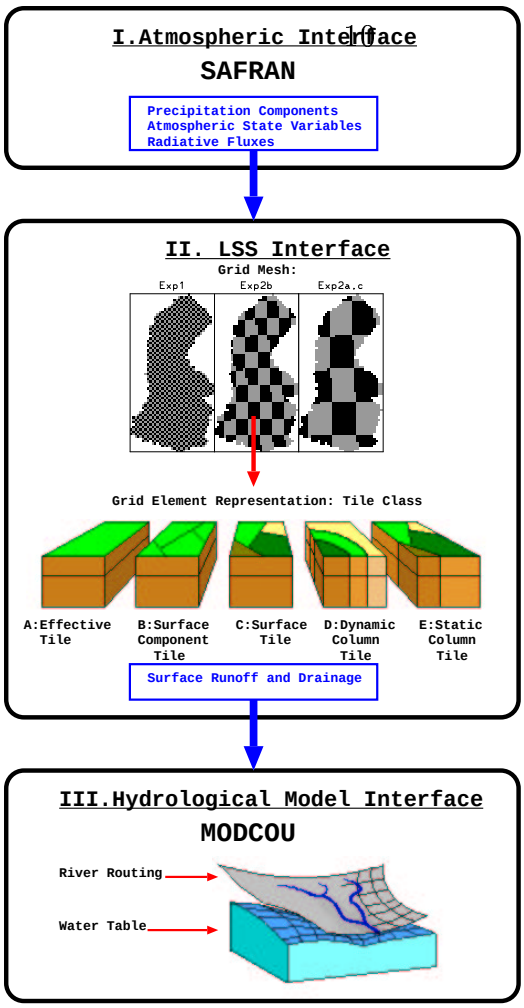

FIG. 2.2. The Rhône modeling system components. The participating LSSs are substituted into the LSS interface (II.) The coupling is one-way, and the variables which are transferred between each component are represented in blue. The LSS grid configuration used for the current study (leftmost: Exp1: 8 km) and a basic representation of LSS-tiling methods are shown.

Four years worth of forcing are used in the current study (1985-89) which coincide with the GSWP (1987-1988) simulations. The four-year annual average solid and liquid precipitation components are shown in Fig. 2.4. Orographic lifting plays a crucial role in precipitation enhancement, while the lowest precipitation values occur near the south-central part of the basin. In addition, there is a significant snow component in mountainous areas (comprising approximately 10% of the total annual basin-wide precipitation). See Etchevers et al. (2001) for further details on the forcing database.

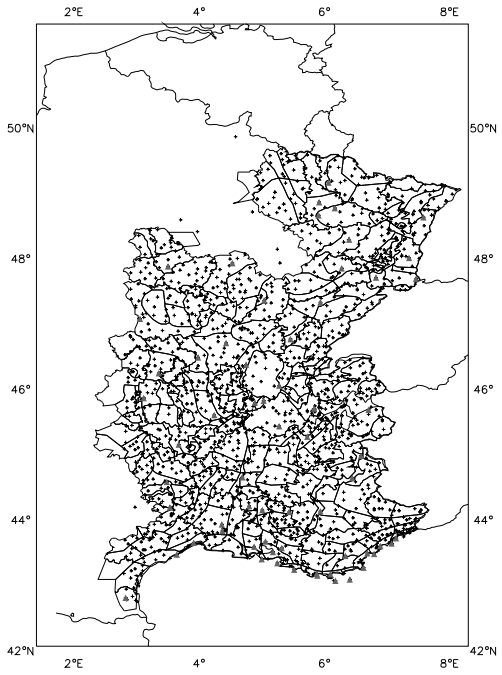

FIG. 2.3. The locations of the meteorological stations used in the SAFRAN analysis (see Etchevers et al. 2001 for details).

The soil parameters are defined using the soil textural properties (described by King et al., 1995). The vegetation parameters are defined using a vegetation map from the Corine Land Cover Archive (Giordano et al. 1990) and a two-year satellite archive of the AVHRR/NDVI Index (Champeaux et al., 2000). There are 10 distinct surface types considered for Rhône-AGG (see Boone et al. 2003 for more details).

2. Hydrological Model

The Rhône modeling system incorporates the distributed hydrological model called MODCOU (Ledoux et al. 1989; Violette et al. 1997). It uses a two-layer approach: the underground (lower of the two) layer encompasses the aquifers for the Rhône and Saône valleys and is active below approximately 21 % of the total surface area of the basin, while the surface layer corresponds to the atmospheric forcing domain and contains 27,054 grid elements (between 1 and 64 such cells are

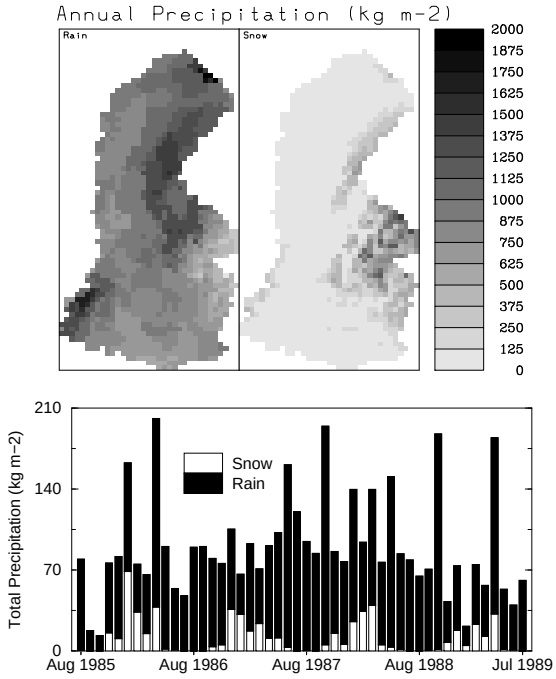

FIG. 2.4. The prescribed total annual snow and rain components averaged over four years (1985-89) are shown in the upper panel over the Rhône basin. The corresponding monthly basin-totals are shown in the lower panel.

within each atmospheric grid box). Topographical data are used to determine the surface hydrographic network and the water transfer time constant between each hydrological grid cell. The water table transmissivity and storage coefficients have been calibrated using the observed streamflow (Golaz-Cavazzi et al. 2001).

3. LSS interface

The function of the LSS interface between SAFRAN and MODCOU is to model the rapid interaction between the atmosphere and the surface through an explicit resolution of the daily cycle, and the slower interaction with the deep soil layers and the hydrological system. LSS output surface runoff is transferred to the surface layer, and routing from each grid cell is based on isochronous zones using a time step of one day. LSS output drainage acts as a source for the water table, which is modeled using the diffusivity equation. There is currently no feedback between the

water table and the LSS. The water table can be either a source or a sink for rivers based on the local water table depth relative to the channel water height.

It is important to note that the other two components of the system (i.e., SAFRAN and MODCOU) have been developed and calibrated independently of any particular LSS, so that different LSSs can easily be inserted into the system. The LSSs which are incorporated into this system for the Rhône-AGG project are listed in Table 2. Further details related to the model coupling can be found in Habets et al. (1999b).

4. Observations for LSS Evaluation

Two sets of observations are used for evaluating model simulations for the Rhône basin. The first consists of 24 daily snow depth observation sites located within the French Alps (circles in Fig. 2.1). These sites are selected from a much larger station database using criteria based on quality control, and by only considering stations with an elevation difference between the site and the grid-box mean altitude of 250 m or less.

The second set of observations consist of daily streamflow data at 145 river gauges which are used for validation of the simulated discharge (filled triangles in Fig. 2.1). Note that for this report, data from 112 basins were used. Based on the work of Etchevers et al. (2001) and Habets et al. (1999b), only basins with surface areas of at least 250 km^2 are used in the modeling system. Damming impacts the flow in some mountainous basins, however, here are a significant number of mountainous basins for which anthropogenic effects are minor or non-existent. Quantitative information on dams is not available (this information is withheld by the French water management agencies), but estimates of such effects are made for some of the larger basins using the observed discharge and the measured precipitation.

CHAPTER 3

RESULTS

This report gives a very general overview of the LSS simulations of the regional scale energy budget and hydrological cycle for the Rhône basin. A more detailed explanation of the causes for LSS model differences can be found in Boone et al. (2003). The LSSs used in the Rhône-AGG and ELDAS experiments (denoted with an $*$) are listed in Table 3.1. Only the Rhône-AGG control experiment was performed by the ELDAS schemes TECMWF, DWD and INM, so that there is no discussion of parameter scaling (Rhône-AGG Exp.s 2 and 3) in this report.

1. Setup

A full set of relatively standard soil and vegetation parameter values was provided to the participants. In addition, the daily discharge for two sub-basins for the four simulation years is provided to the participants for an optional calibration of hydrological-model parameters (see Boone et al., 2003, for more details). The forcing variable definitions, sign conventions and units follow the Assistance for Land-surface Modeling Activities (ALMA: Polcher 2001), data convention which has been set up as a part of GLASS, and they are used throughout this report (see Appendix A for a listing). Also see http://www.cnrm.meteo.fr/mc2/projects/rhoneagg/ for more details about the Rhône-AGG setup and ALMA convention.

TABLE 3.1. LSS Listing. ELDAS models are indicated using an $*$.

Acronym	ID	Name	reference
ISBA$*$	A	Interactions between Soil Biosphere Atmosphere	Noilhan and Mahfouf (1996)
ECMWF$*$	E	European Centre for Medium-Range Weather Forecasts scheme	Van den Hurk et al. (2000)
MECMWF$*$	H	Modified ECMWF scheme	Van den Hurk and Viterbo (2002)
DWD$*$	W	German Weather Service Multi-Layer Soil Model	Schrodin and Heise (2001)
TECMWF$*$	T	Modified ECMWF scheme	Van den Hurk and Viterbo (2002)
INM$*$	I	ISBA-HIRLAM	Rodríguez et al. (2003)
NOAH	B	NOAA/National Centers for Environmental Prediction	Chen et al. (1997)
COLA	C	COLA/SSiB (Simple Biosphere Model)	Xue et al. (1991)
MOSES-PDM	D	Met. Office Surface Exchange Scheme Probability-Distributed Moisture	Essery et al. (2003)
NSIPP	F	NASA Seasonal-to-Interannual Prediction Project & Catchment model	Koster et al. (2000)
VIC	G	Variable Infiltration Capacity Model	Liang et al. (1994)
SWAP	S	Soil-Water-Atmosphere-Plants	Gusev and Nasonova (1998)
VISA	J	Versatile Integrator of Surface-Atmospheric processes	Yang and Niu (2002)
SPONSOR	K	Semi-distributed ParameterizatiON scheme of ORography-induced hydrology	Shmakin (1998)
CLASS	L	Canadian Land Surface Scheme	Verseghy (2000)
ORCHIDEE	M	LMD surface model	de Rosnay and Polcher (1998)
SIBUC	N	Simple Biosphere model including Urban Canopy	Tanaka et al. (1998)
CHASM	O	Chameleon Surface Model	Desborough (1999)

A basic LSS classification scheme was used in the Rhône-AGG experiment. They were classified based on: i) whether they used a tile or effective surface approach, ii) snow scheme complexity (a soil-vegetation-snow composite or an explicit

snowpack), and iii) sub-grid runoff parameterization (if any). The LSS configurations used for Rhône-AGG are listed in Table 3.2. See Boone et al. (2003) for further details about the classification scheme. Note that the DWD LSS does not use a sub-grid runoff scheme, but significant surface runoff can be generated before saturation of the soil column (unlike in ECMWF or INM for example) owing to another mechanism (thus the $*$ in Table 3.2). For positive soil moisture tendencies, a reduction factor is applied to those tendencies if the moisture exceeds the field capacity, and the runoff is then adjusted accordingly (Martin Lang, pers. commun.). It will be shown that this method generates surface runoff with magnitudes comparable to those of LSSs with sub-grid runoff schemes.

TABLE 3.2. The LSS configurations for Rhône-AGG. The r subscript represents a rerun. The type of surface [effective (Efc) or tile], the snow scheme [explicit (E) or composite (C)], the number of active thermal (N_T) and hydrological (N_w) layers, the basin average soil depth (d_{soil}: m), and the type of sub-grid runoff (SGR) scheme (if any) are listed. See Boone et al. (2003) for further details.

LSS	Surface	Snow	N_T, N_w	d_{soil}	SGR
ISBA	Efc	3E	2, 3	2.43	VIC
ECMWF	Tile	1E	4, 4	2.89	none
MECMWF	Tile	1E	4, 4	2.89	Arno-TOP
TECMWF	Tile	1E	4, 4	2.89	Arno-TOP
DWD	Efc	1E	7, 7	7.29	none$*$
DWD$_r$	Efc	1E	7, 7	7.29	none$*$
INM	Tile	C	2, 2	2.43	none
INM$_r$	Tile	C	2, 2	2.43	VIC

2. Simulations

25 baseline simulations were done by 18 participant models, and 7 of these LSSs elected to perform reruns for various reasons. A summary of the reruns performed for Rhône-AGG is given in Boone et al. (2003). In terms of the ELDAS model reruns, the DWD model made some modifications to their model hydrology, notably

the snowpack module: a snow ageing process was added (impacting the albedo), the snow density limits were changed (from 500/800 to 150/400 kg m^{-3}), and the snowpack melting algorithm was improved. The INM model incorporated a simple sub-grid runoff parameterization based on that of the ISBA scheme (Habets et al. 1999a). The TECMWF is essentially a rerun of the MECMWF, except that the soil parameter model of Clapp and Hornberger (1978) replaced the Van Genuchten (1980) model, and the sub-grid runoff scheme was modified in order to limit runoff in areas of low topographic variability (compared to the MECMWF run). The first year (ending July 31, 1986) is treated as a spin-up year, so that only the results for the final three years are analyzed in this study.

a. Energy and Water Balance

The LSS-simulated 3-year basin-wide average water fluxes, SWE (snow water equivalent), and turbulent energy fluxes are shown in Fig. 3.1.

There is a reasonable overall agreement in terms of the total evaporation simulated by the LSSs (Fig. 3.1a), with a range of approximately $\pm$ 12% (with the exception of SIBUC and the ORCHIDEE baseline run). However, the partitioning varies greatly among the schemes even though the most significant soil and vegetation parameters were prescribed. Transpiration (TVeg) is the dominant component for most LSSs, while ECanop and ESoil vary more significantly from one scheme to another. Sublimation is approximately negligible for all of the LSSs. This partitioning has a profound effect on the simulations in terms of soil moisture and runoff (this will be discussed more in subsequent sections).

In terms of the ELDAS models, the ECMWF-based LSSs have the largest TVeg, while the other models simulate a more comparable amount. In contrast, DWD simulates the most ESoil. The other notable difference is between ISBA and INM: INM simulates significantly more ECanop. This is most likely a result of the

fact the INM used LAI values from a different database than that provided to the other pariticpants (i.e. INM used it's own LAI database). Other reasons for this discrepency are probably related to the differences in the water interception coverage formulation (which is different over forested regions where ECanop is generally the largest), although differences arising to the use of multiple tiles (by INM) are possible (e.g. owing to large roughness lengths over forested regions compared to ISBA). Note that only the grid-box average fluxes were reported, so that a further investigation of such differences is beyond the scope of this report. The large ECanop is significant in that this water never interacts with the soil, so that a larger ECanop (with nearly the same overall Evap) implies drier soils and lower runoff. INM and ISBA have nearly the same total transpiration abd evapotranspiration, but the paritioning between ESoil and ECanop is significantly different.

Evapotranspiration (latent heat flux) dominated the turbulent transfer (Fig. 3.1c) for all but one LSS overall, and for all of the ELDAS schemes. DWD simulates the lowest Bowen ratio: less than approximately 0.10 for the basin as a whole. In terms of an annual average, the LSSs generally simulate significant sensible heat fluxes over the central valley and the southern zones (the largest values). The total turbulent flux simulated by the ELDAS schemes is consistent with the majority of the other LSSs, falling between approximately 50 and 60 W m^{-2}.

The runoff components are shown in Fig. 3.1b. Generally speaking, drainage is larger than surface runoff, although there is almost no overall agreement in the partitioning. This partitioning has an impact on the discharge simulation, especially for smaller-scale basins as surface runoff has a fast time response compared to drainage. This will be discussed further in the section on the river discharge simulation.

The SWE (Fig. 3.1d) varies greatly across the LSSs. Models can be classified into essentially two groups: models with composite snow schemes generally have

relatively low SWE values (e.g.s NOAH, MOSES, INM), while the explicit schemes tend to have the highest values (e.g.s ISBA, VISA, SWAP). For further details about the LSS snow-scheme classification, see Boone et al. (2003), which was based on the work of Slater et al. (2001). Note that NSIPP simulated a very large SWE compared to the other LSSs, but the snow module has since been updated to give lower SWE estimates (Koster, personal communication).

The three-year average evapotranspiration (Evap) is shown as a function of space in Fig. 3.2. Most of the LSSs simulate the least Evap over the mountainous areas, mostly owing to the significant snow cover. The largest Evap is found in the valley region, although there is a great deal of spatial variability among the schemes. In terms of the ELDAS models, DWD simulates areas of relatively high Evap, while INM tends to have the lowest Evap in the valley regions. This difference arises primarily due to the relatively large (compared to most LSSs) baresoil evaporation simulated by DWD (see Fig. 3.1a). Finally, INM has the largest Evap in mountainous regions for relatively high elevations, owing to it's relatively sparse snow cover.

The three-year average surface runoff (Qs) and drainage (Qsb) are shown in Fig.s 3.3-3.4, respectively. The LSSs all simulate the same general total runoff (i.e. Qs+Qsb) pattern, with the largest runoff in mountainous regions, and the least along the Mediterranean coast. This is consistent with the spatial precipitation distribution shown in Fig. 3.14, and the relatively large water release due to snowmelt in the Alps. In terms of the ELDAS models, ECMWF and INM have no subgrid runoff and therefore Qs is negligible at nearly all of the gridpoints. TECMWF has a slight reduction in Qs compared to MECMWF, which is mainly related to the re-computation of the sub-grid runoff parameters (based on topography). ISBA and DWD have similar patterns (with significant runoff occurring both over the Alps and the Vosges), although with a different magnitude. The INM_rerun shows some

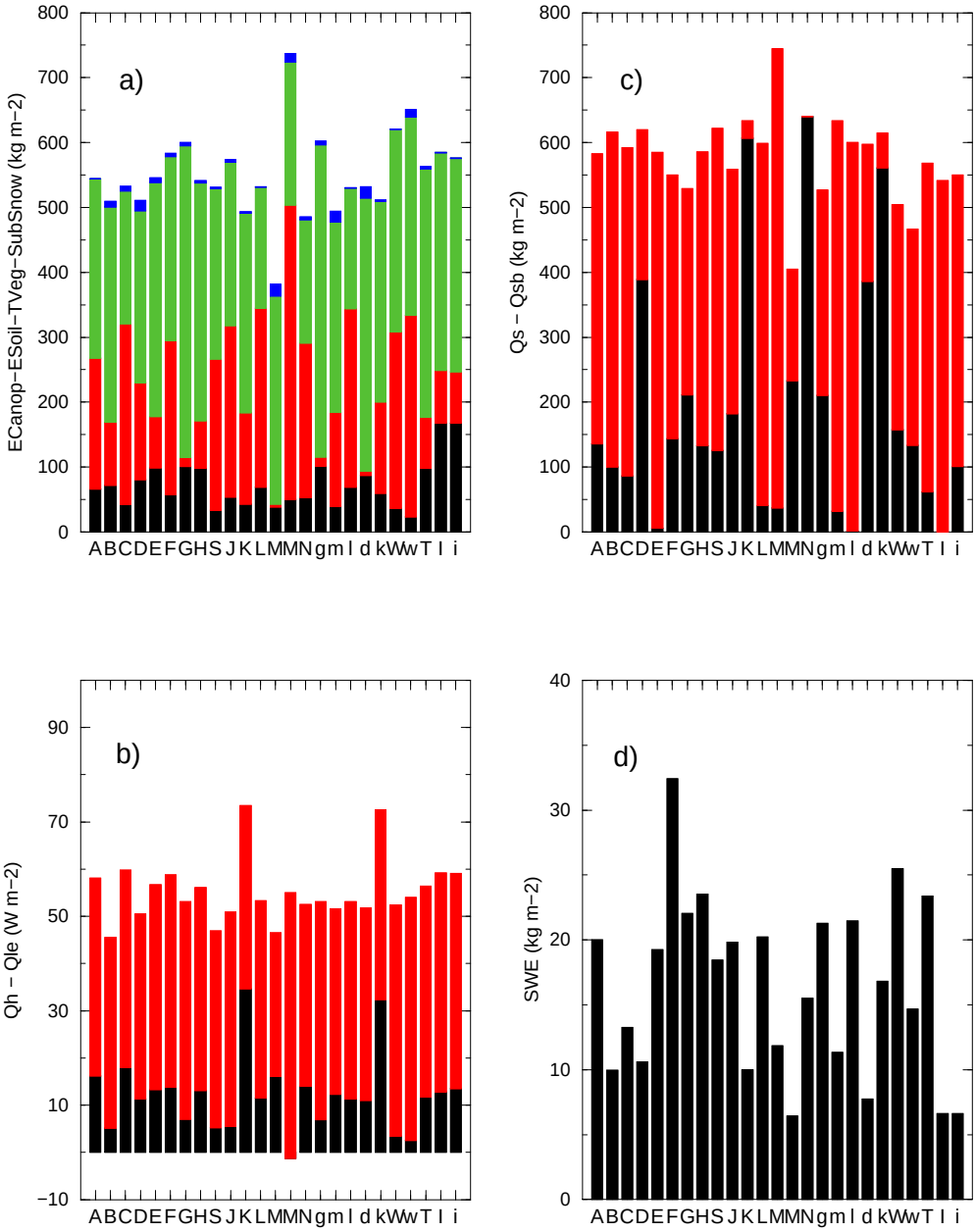

FIG. 3.1. The three-year basin-wide average evapotranspiration (a), turbulent flux (b), and runoff (c) components are shown, along with the SWE (d). LSS IDs are shown in Table 3.1.

increases in Qs compared to the baseline run, but relatively little over the Alps

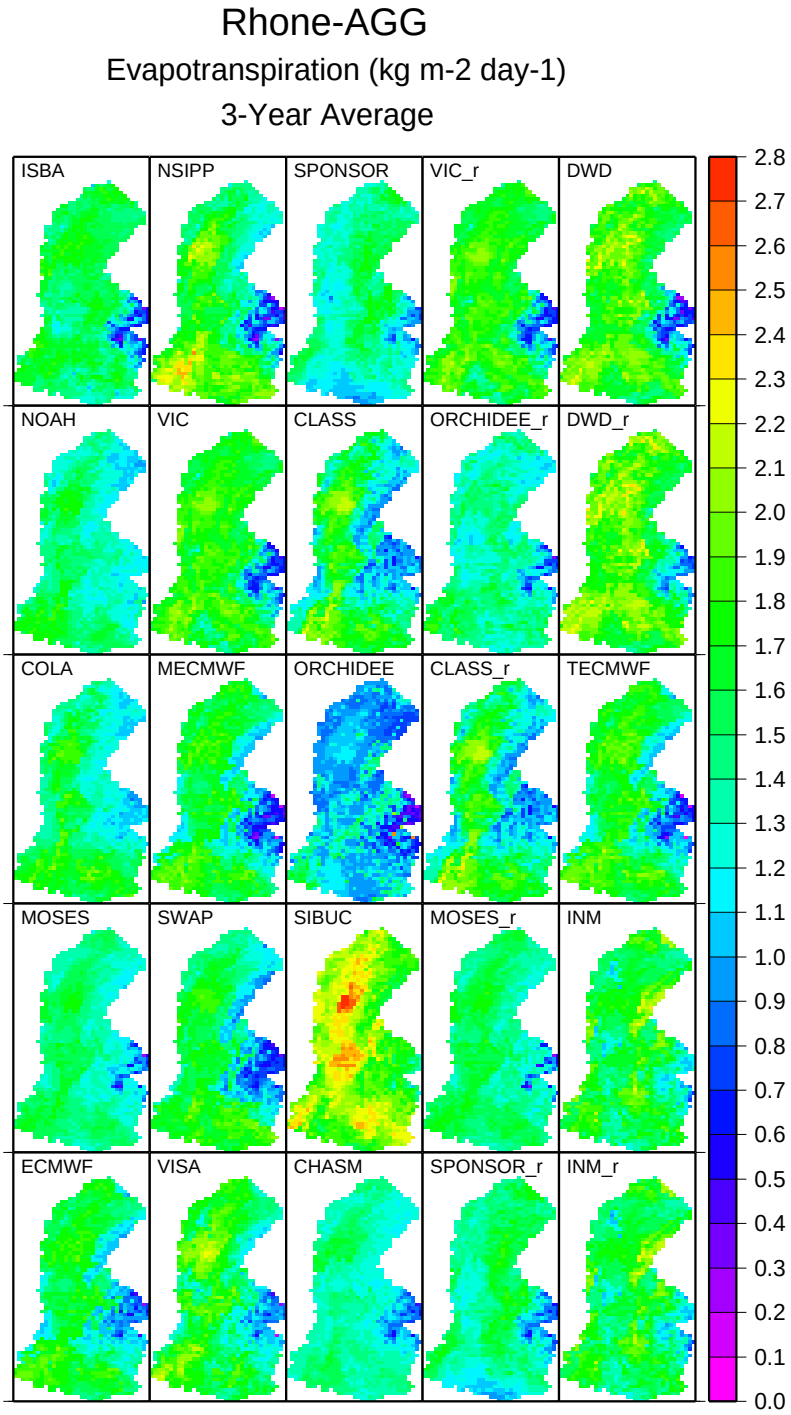

FIG. 3.2. The three-year average evapotranspiration (Evap).

(compared to the other LSSs): this seems to be, once again, related to the rather low simulated snow accumulation in the Alps.

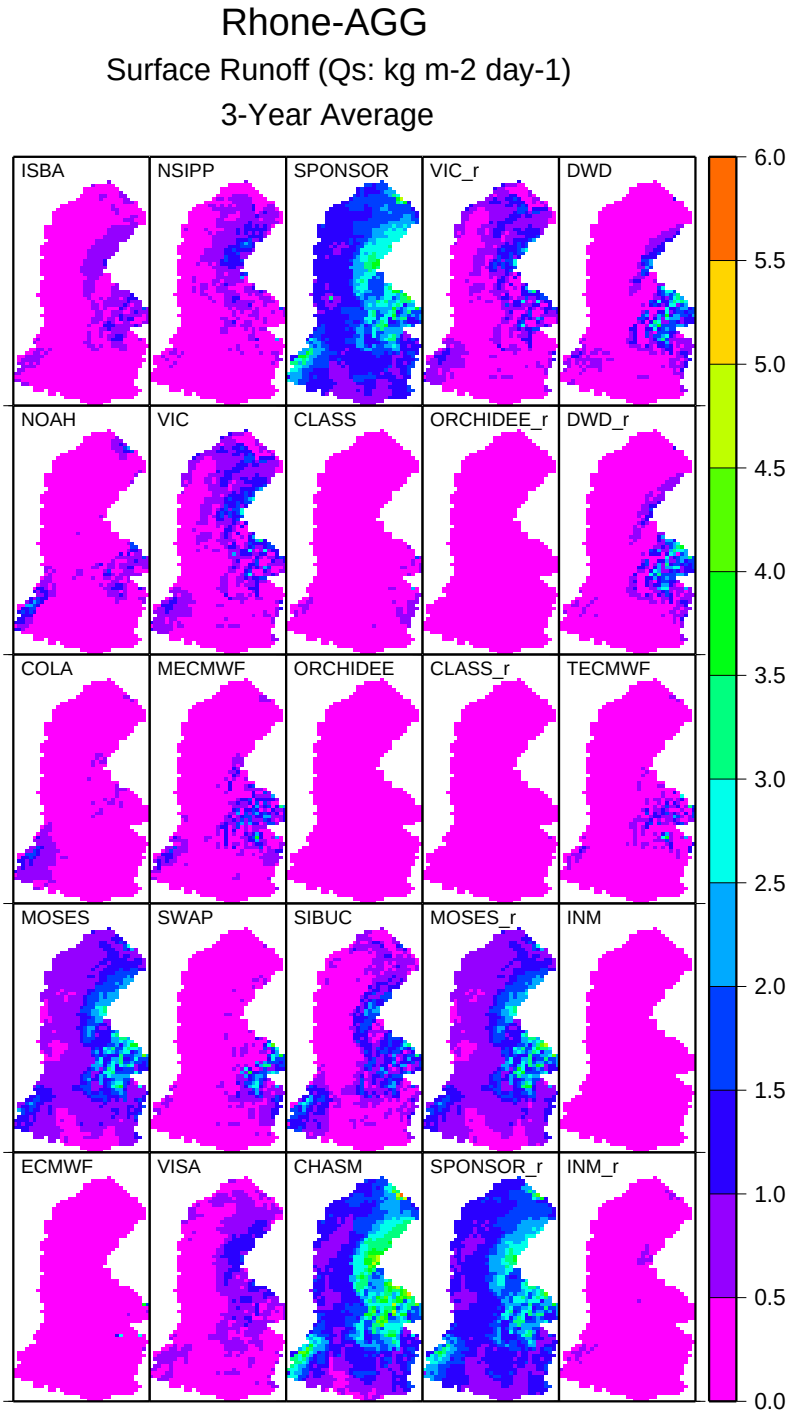

FIG. 3.3. The three-year average surface (overland) runoff (Qs).

The basin-wide 3-year average monthly runoff components and evapotranspiration are shown in Fig. 3.5. The purpose of this plot is to highlight temporal differences in the water sinks. Several differences can be noted among the ELDAS

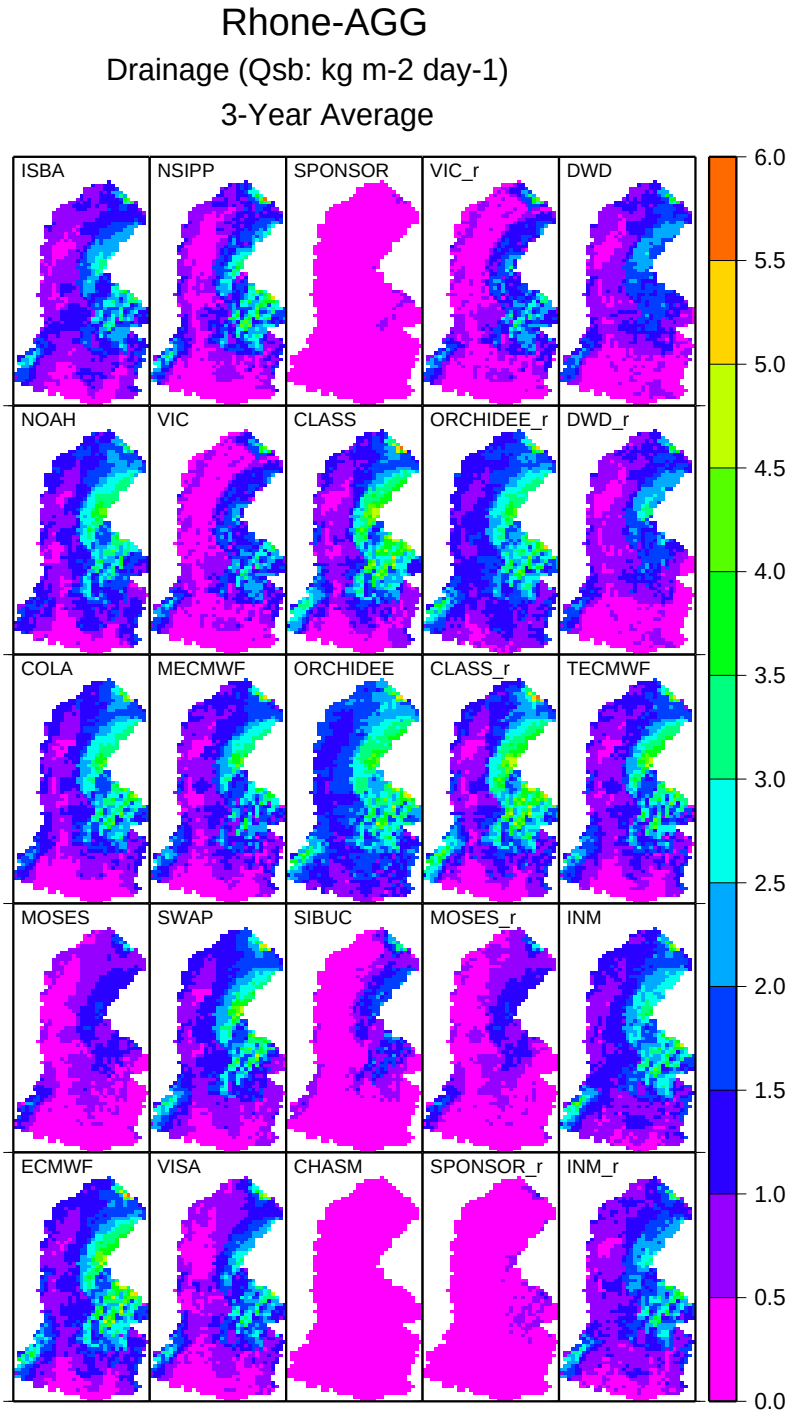

FIG. 3.4. The three-year average drainage or baseflow runoff (Qsb).

models. The ISBA Evap is water-limited in the summer and early fall to the largest degree, while DWD is limited the least. Not surprisingly, all of the schemes have similar Evap predictions in the winter, as Evap is primarily controlled by (weak)

atmospheric demand. In terms of runoff, all of the ELDAS models capture the autumnal soil water recharge (compared to CHASM, ORCHIDEE and SPONSOR which do not): i.e. moderate runoff despite the most significant precipitation of the entire year. DWD has the lowest winter drainage runoff as the soil is deeper and therefore has a larger storage capacity (more potential recharge after the relatively dry summer), and because it has the most significant surface runoff component. TECMWF has the smoothest overall runoff response: it is the least responsive to precipitation events. All of the ELDAS schemes simulate the largest runoff in spring, although with differences in magnitude and partitioning. INM_rerun and ISBA have similar runoff fluxes, although ISBA has a slighly larger surface runoff ratio. This seems to be related to the larger ECanop of INM, and in spring, due to the larger snowmelt simulated by ISBA.

The basin-wide 3-year average monthly surface energy budget components are shown in Fig. 3.6. The Rnet among the ELDAS models is most similar between ISBA and TECMWF, with a nearly zero flux in the winter. The DWD LSS has a negative Rnet in winter, with the latent heat flux energy being mostly provided by atmospheric heat. ISBA has the largest peak sensible heat fluxes in the summer, which is related to the water-limited evapotranspiration (as previously discussed). All of the ELDAS-LSSs have an approximately zero net ground heat flux over the 3-year integration except for INM: ground heat flux is positive for all months of year but one, which is a bit surprising for a three-year period (as it is the only LSS to simulate this behavior), but note that the energy balance is maintained.

1) Soil Moisture

A very important aspect of the LSSs is the simulation of the soil moisture, as this variable is generally the most important land surface variable. It has been recognized that, however, soil moisture is not simulated in a consistent manner among

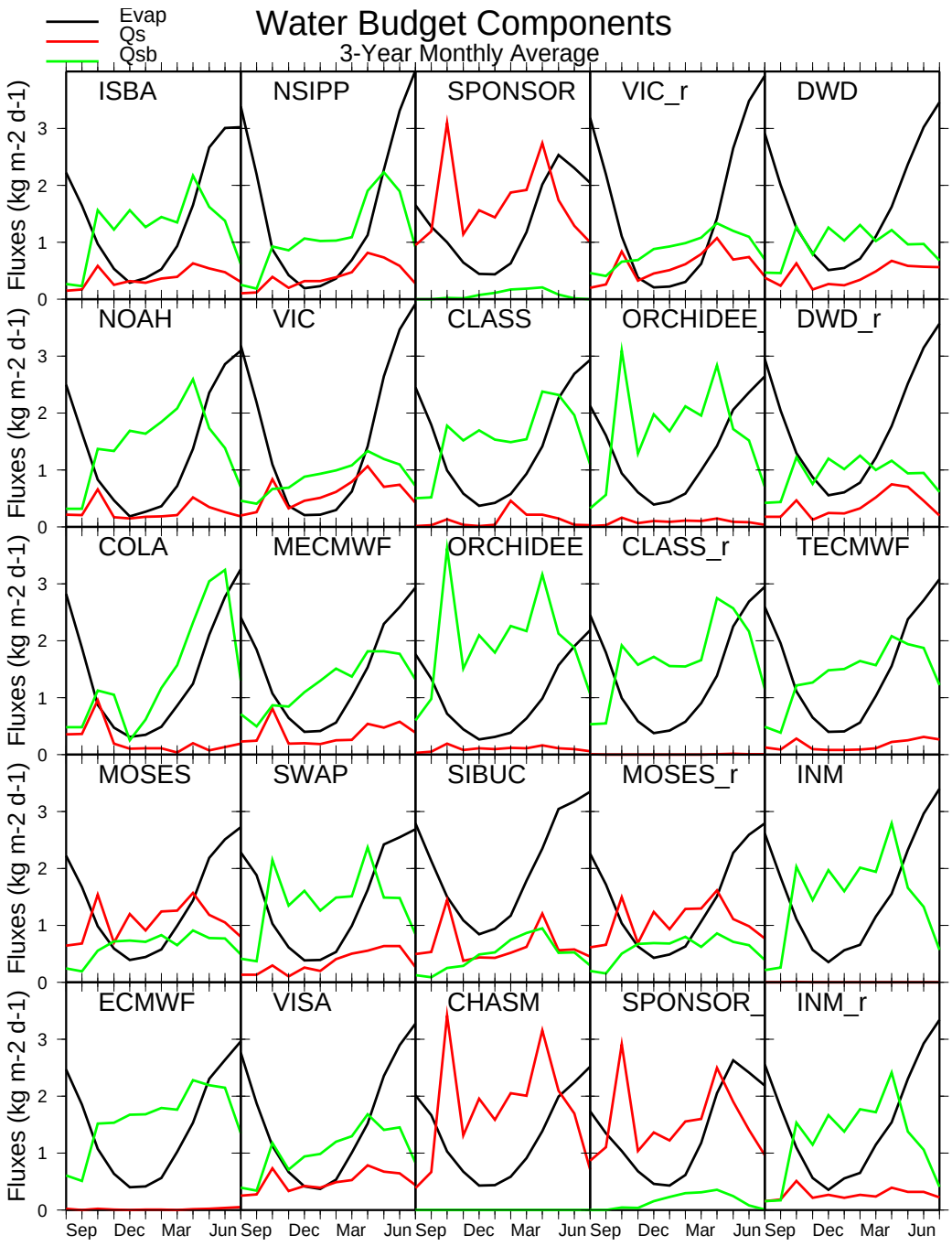

FIG. 3.5. The basin-wide 3-year average monthly runoff components and evapotranspiration (units of kg m^{-2} day^{-1}.

LSSs (e.g.s Shao and Sellers, 1996; Entin et al. 1999). In order to facilitate the inter-comparison of this variable, several soil moisture indices have been established.

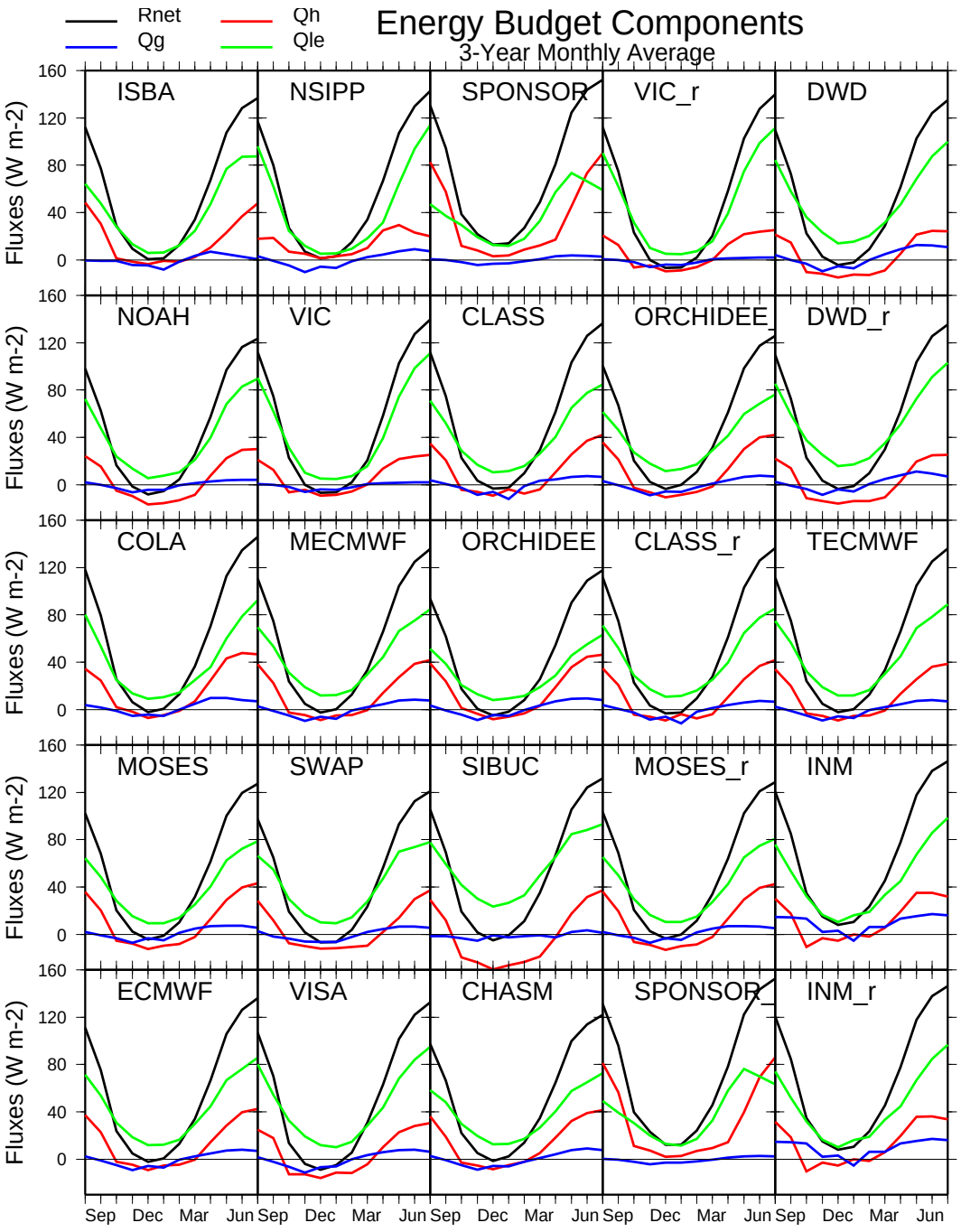

FIG. 3.6. The basin-wide 3-year average monthly surface energy budget components.

In this study, we examine the soil wetness index (SoilWet), defined as

$$\mathrm{SWI} = \frac{W/\left(d_{soil}\,\rho_w\right) - w_{\mathrm{wilt}}}{w_{\mathrm{max}} - w_{\mathrm{wilt}}} \qquad (\mathrm{SWI} \le 1) \quad ,$$

where W represents the total soil water content (kg m^{-2}) for the layer thickness d_{soil} (m), ρ_w is the density of liquid water, and w_{wilt} represents the wilting point volumetric water content (m^3 m^{-3}). The maximum volumetric water content (w_{max}) is equivalent to the porosity (w_{sat}) for all of the schemes but two, ORCHIDEE and CHASM, which assume $w_{\text{max}} = w_{\text{fc}}$. Values of the basin-average total soil depth (d_{soil}) for each LSS are listed in Table 3.2.

The 3-year average SWI is shown in Fig. 3.7. The spatial pattern is generally similar among the ELDAS LSSs (and generally all LSSs): the wettest soils are found in the north-east, and the driest soils are located along the southern zone. But the magnitudes are quite different, which occurs despite the fact that most models used the same soil (and vegetation) parameter values and depths. Koster and Milly (1997) attributed this difference in soil water storage equilibrium to the scheme-dependent interplay between the runoff and evapotranspiration formulations. INM and ISBA are quite similar, which is not surprising as the equilibrium value of the soil moisture is strongly modulated in these schemes by the value of the field capacity parameter (and they both use the Force-Restore approach: see Noilhan and Mahfouf, 1996).

A closer inspection of the spatial patterns, however, yields some differences. DWD and TECMWF have similar overall magnitudes, although TECMWF has a zone of dry soils in the Rhône valley, while DWD simulates dry soils over a zone east (and slightly higher) of the north-south axis of the valley, and over some areas in the Alps (similar to ISBA). Also, none of the ELDAS schemes assume a saturated fraction of the surface in terms of the evaporation computation: it is only used for runoff generation. The two schemes which do include saturated areas for the evapotranspiration computation (NSIPP and VIC) have the largest SWI range in terms of spatial variability.

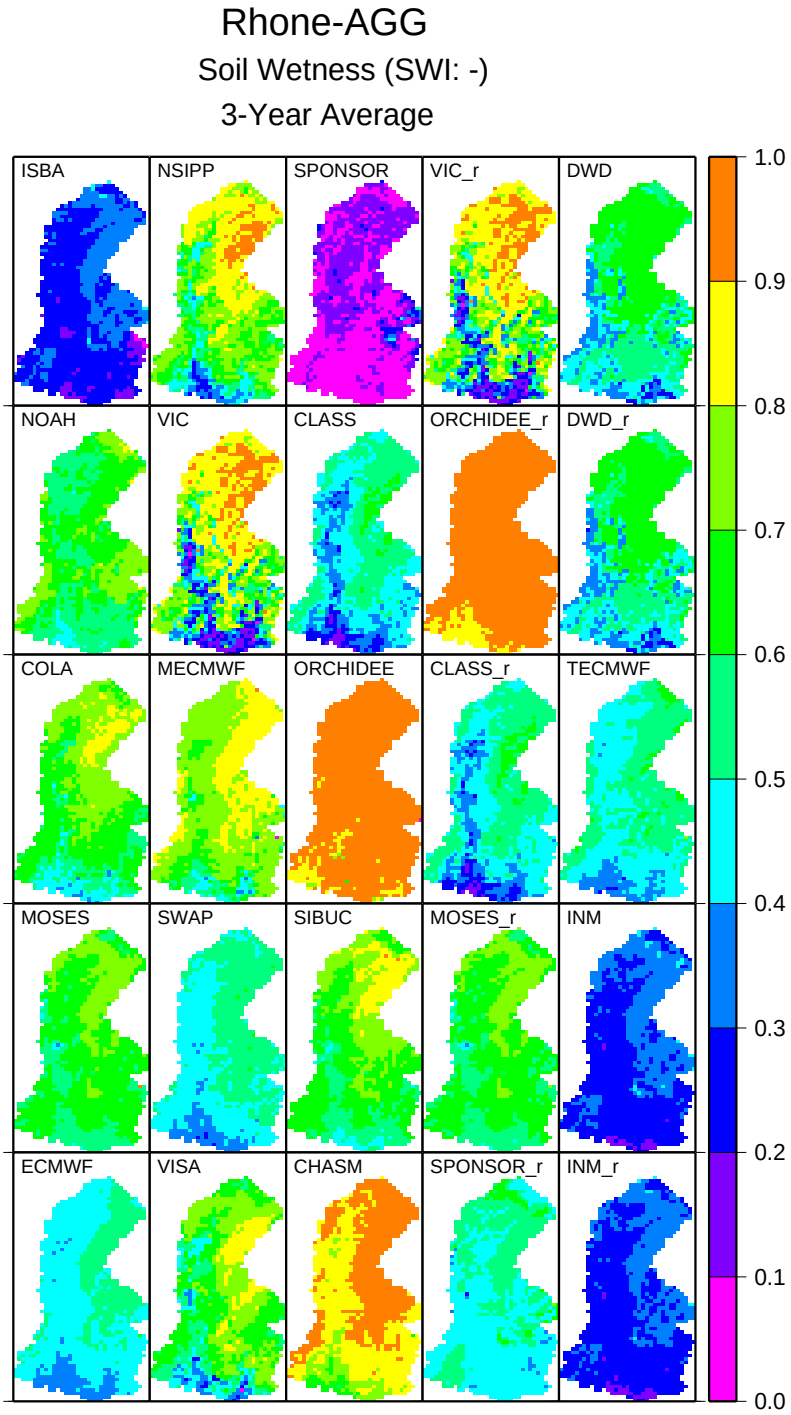

FIG. 3.7. The 3-year average SWI (SoilWet: soil wetness index).

The basin-scale three-year average daily SWI is shown in Fig. 3.8. Soil water recharge occurs in fall, with a general leveling off of soil moisture in the winter as most soils are near their effective field capacities. The term "effective" is used

here as the Richard-equation water-movement based LSSs (all but ORCHIDEE, CHASM, ISBA and INM) have no direct dependence on the field capacity parameter (except possibly for the influence of water-stress on transpiration). Such LSSs (ELDAS: ECMWF schemes, and DWD) seak out an equilibrium state which can be more variable on a year to year basis and is more dependent on the runoff and evapotranspiration formulations. In spring and early summer, soil water drops due to evapotranspiration until a water-limited level is reached.

Despite the highly variable absolute values of the soil moisture, the phase and amplitude of the actual soil water change is quite similar among most LSS. The mean SWI value for each LSS has been removed in Fig. 3.9, and the LSS-average time series is shown as a reference (in red). The ELDAS schemes are quite similar in terms of SWI change. DWD has a slightly lower amplitude and lagged response compared to the other ELDAS-LSSs, but this is expected due to the larger soil depth used by this model. This plot shows that, on average for the entire basin, the change in water storage is actually quite similar among the schemes (most LSSs used the same or similar total soil depths and parameters), despite the temporal differences in the evapotranspiration and the runoff fluxes (e.g. see Fig. 3.5).

b. Snow Simulation

The three-year average SWE spatial distribution is shown in a zoomed-in portion of the Rhône basin in Fig. 3.10. The average SWE over the Vosges (north-eastern part of the basin) and the Cevennes (south-west) was significantly less, and the snow depth observation network is located in the Alps, so that only the SWE over the Alps is discussed in this report. All of the LSSs used the prescribed snowfall, which is strongly modulated by the basin topography. MECMWF tends to accumulate more snow than DWD and ISBA, while INM simulates by far the least.

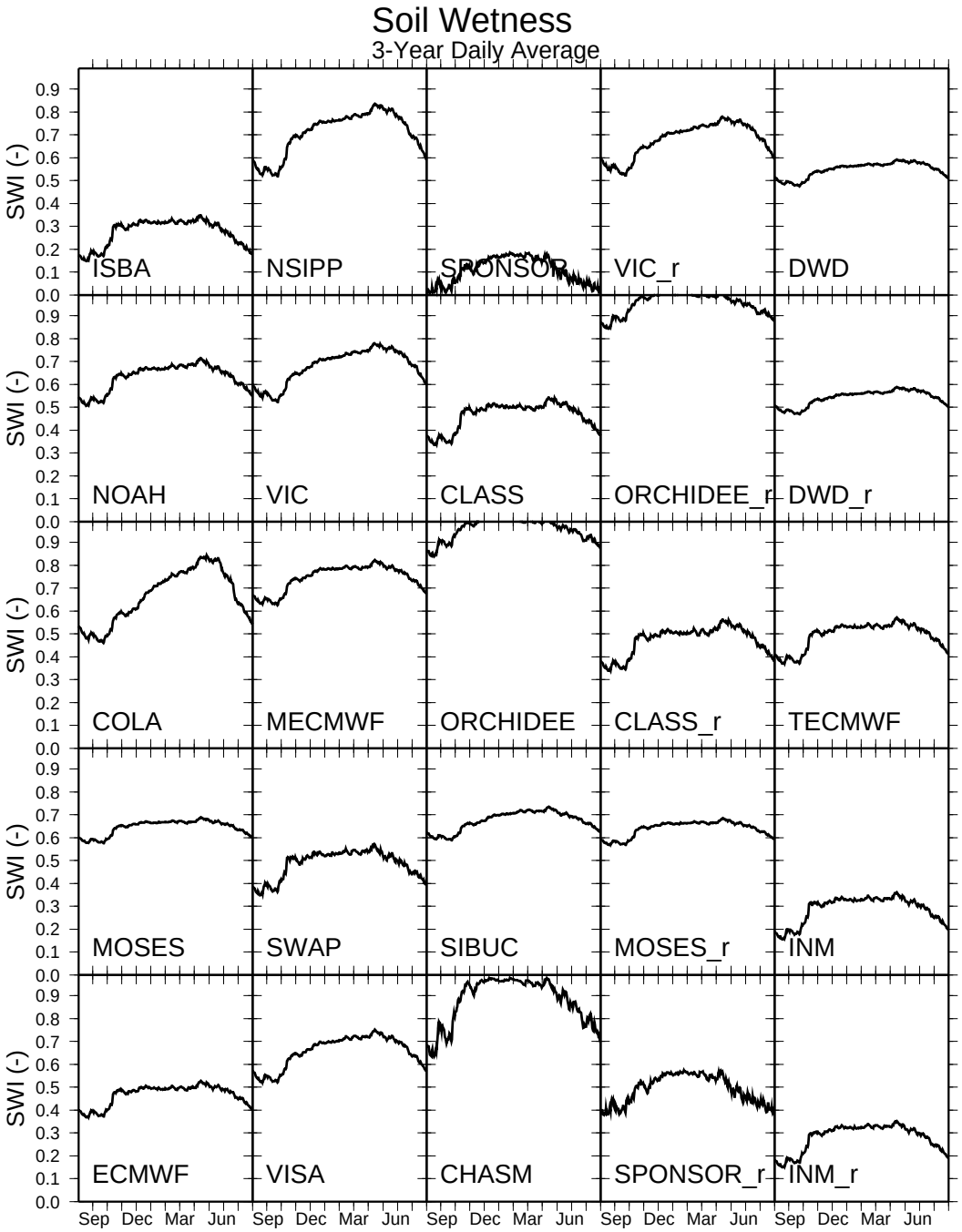

FIG. 3.8. The basin-scale three-year average daily SWI.

This means that INM tended to melt more snow during the winter months, leading to a shorter duration and lower total accumuation.

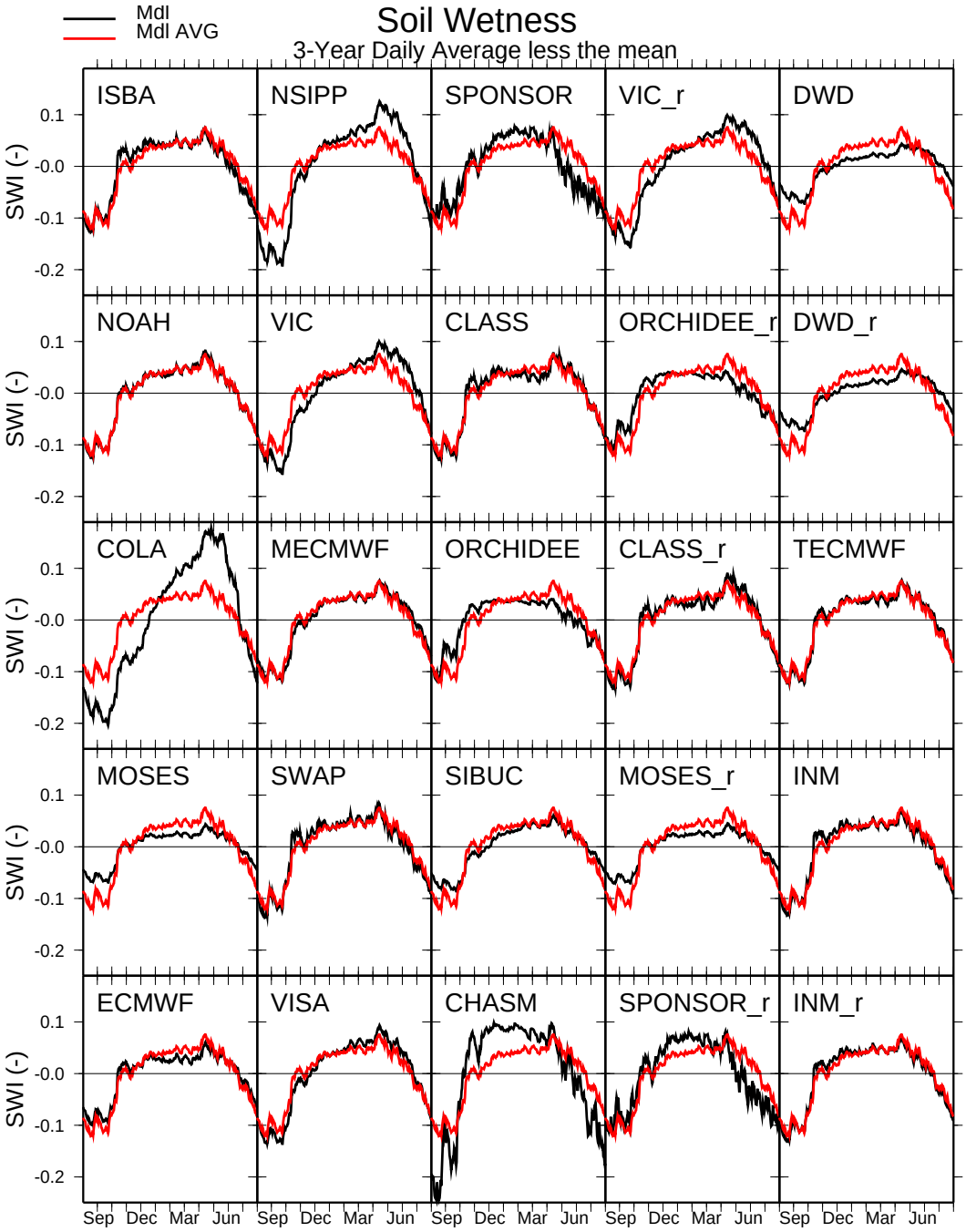

FIG. 3.9. As in Fig. 3.8, except the spatial and temporal mean value has been removed. The LSS-average time series is shown as a reference (in red).

In terms of comparison with observations, a summary of the snow depth simulation for the 25 model simulations is shown in Fig. 3.11. Statistics were computed

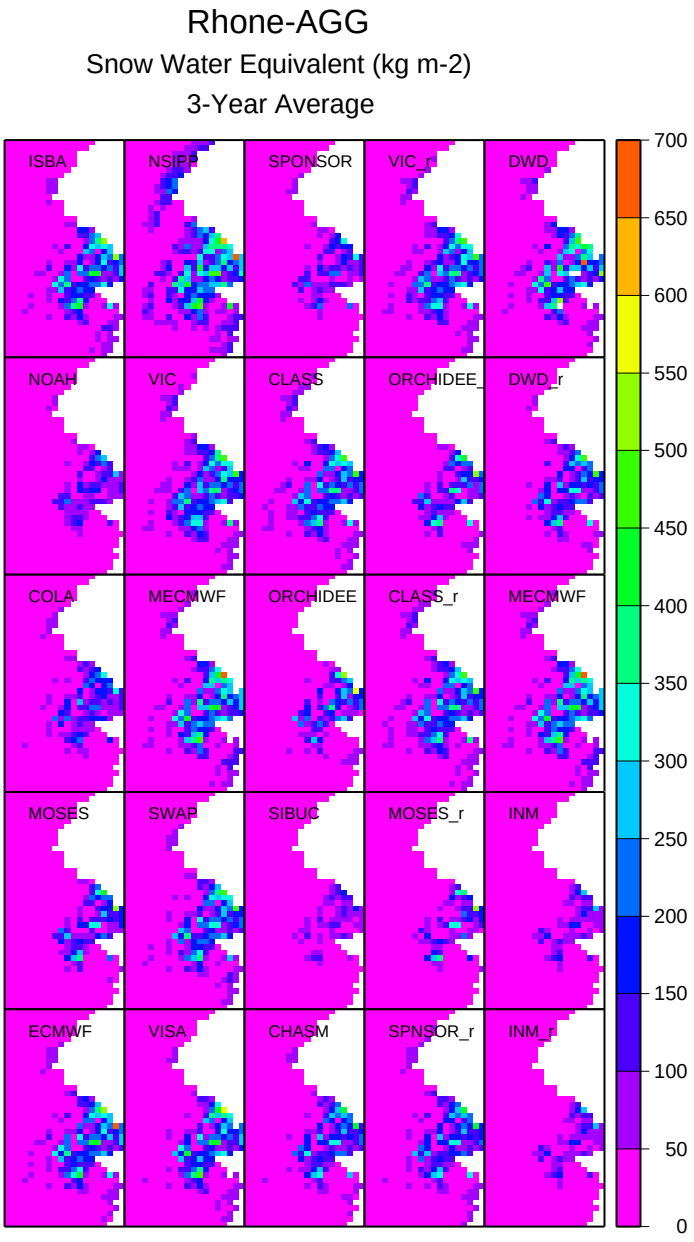

FIG. 3.10. The 3-year average SWE (kg m^2) in a zoomed region of the Rhône basin.

using the daily observed and simulated snow depths for 24 snow sites (see Fig. 2.1 for locations) over a 3-year period.

The ISBA model had among the best overall snow simulations, and the best simulation for the ELDAS models, but it is the only LSS using a multi-layer explicit

snow scheme (Boone and Etchevers, 2001). As discussed in Boone et al. (2003), explicit snow schemes performed the best overall. The ECMWF also performed relatively well, and it uses a snow-devoted tile (the energy budget is not a composite). The TECMWF scheme (which has nearly the same snow model) performed nearly the same, except that it tended to accumulate slightly more snow, especially at higher altitudes. This most likely arises due to the fact that TECMWF (and MECMWF) reduces the surface roughness in response to snow cover compared to ECMWF, thus resulting in less ablation but also less melting due to lower heat (turbulent) transport from the atmosphere to the snowpack.

The DWD significantly over-estimated the snow depths (and the SWE) in their baseline run, however significant improvements were made to the snow scheme for the DWD_rerun in terms of the SWE (see Fig. 3.12). Note that at the time of the writing of this report, the DWD-simulated snow depth and snow density variables were not available, so that a fixed snow density value (250 kg m^{-3}) was used to diagnose snow depth from the SWE. A constant density will generally cause an underestimate of snow depth early in the season, and an overestimate late, and less depth variability (mostly owing to significant snowfall events, especially over relatively shallow existing snowpacks). The use of a constant snow density, therefore, will cause a slight degradation of snow statistics compared to a time-varying value (so one would expect slightly improved snow statistics for the DWD model if a reasonable time-varying snow denisty replaced the constant value). The INM scheme is a composite snow model. As is the case for similar such models (e.g. NOAH, ORCHIDEE...), the snow depth was greatly underestimated, even if a very low snow density was imposed. Such schemes were found to significantly over-estimate winter and early spring melt events for the Rhône basin (Boone et al. 2003).

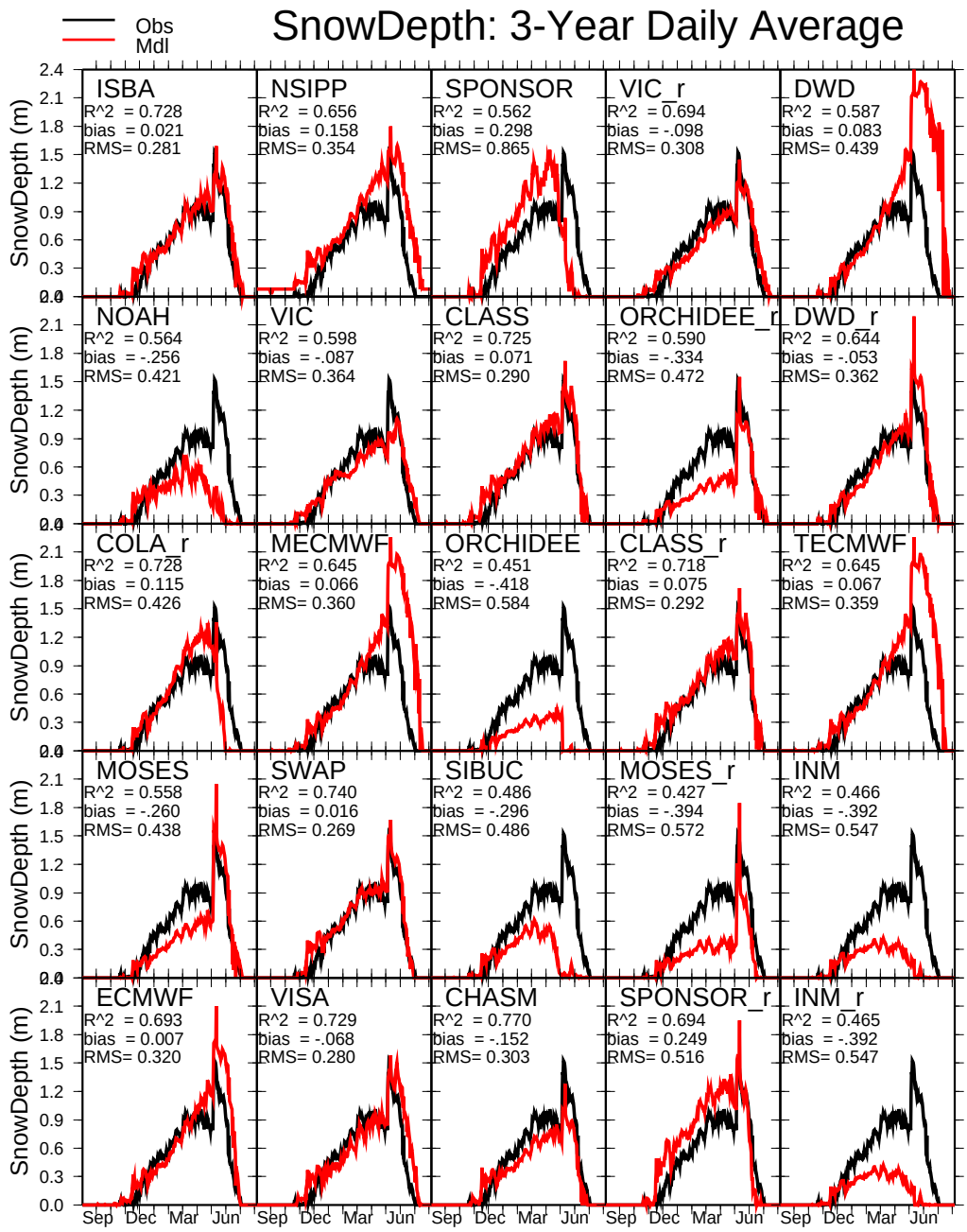

FIG. 3.11. The observed (black) and simulated (red) snow depth for 25 LSS realizations. The annual cycle averaged over 3 years is shown. The data points and simulations are averaged over the 24 sites: the statistics are calculated over all of the sites over 3 years at approximately 1-day intervals. The root mean square error (RMS in m), squared correlation coefficient (r^2) (see Appendix B), and the bias (m) are shown.

A comparison of the basin-average three-year average monthly SWE is shown in Fig. 3.12. The SWAP simulation (the best statistically) is shown as a reference

in red. As it turns out, the schemes which simulated the best snow depth also simulated very similar SWE (e.g. ISBA, SWAP, VISA, CLASS). Their physics are also similar: all had at least two snow temperatures and explicit snow covers. Most of the LSS with composite snow models are easily identified (e.g. NOAH, INM, MOSES, ORCHIDEE).

c. River Discharge

The daily discharge was computed for all of the LSSs over a three-year period for 145 basins of varying sizes within the Rhône basin. Only basins with surface areas in excess of 250 km^2 were treated. 112 of these basins had enough observational data to make statistical evaluations.

1) Rhône-AGG special basins

Four basins were analyzed in detail for the Rhône-AGG experiment (see Fig. 2.1): Saone at Lechatelet (with an area of 11,700 km^2), Ardeche at Sauze-St.Martin (2,240 km^2), Durance at LaClapiere (2,170 km^2), and the Rhône at Viviers (70,100 km^2). The simulated and observed monthly average discharge (averaged over 3 years) is shown for the Rhône at Viviers in Fig. 3.13. Note that the shown statistics were computed using the daily values. This station represents roughly 80 % of the entire basin.

The Force-Restore soil hydrology schemes (ISBA and INM) performed comparably, which is not surprising given that INM is also based on the ISBA model. The INM_rerun (with the addition of sub-grid runoff) is slightly better than the baseline run for this basin: but in fact it will be shown that sub-grid runoff is especially important for smaller-scale basins (and differences between the INM-INM_rerun and ECMWF-TECMWF runs becomes more marked).

The ECMWF and TECMWF schemes also perform similarly, with a slightly lower runoff response in winter. This is partially related to the fact that this LSS

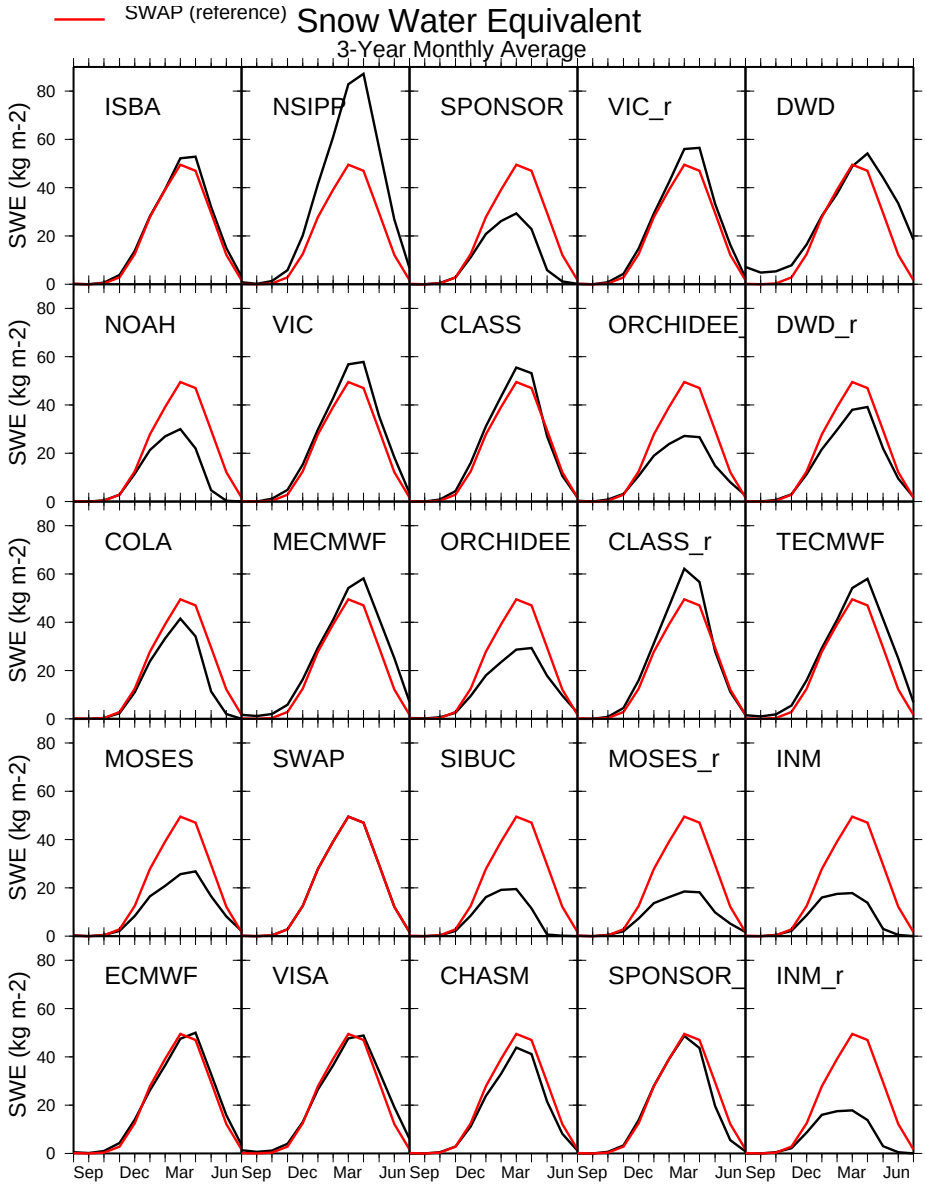

FIG. 3.12. The 3-year average monthly SWE simulated by the LSSs (black). Note that the SWAP simulated SWE (red) is shown as a reference.

uses a fixed soil depth (2.89 m) which is slightly larger than the basin-average value used by most LSSs (2.43 m), thereby causing the model to retain more water. The large winter precipitation amounts can be seen in Fig. 3.14. The DWD scheme, which extends very deep into the soil, has the weakest winter-runoff.

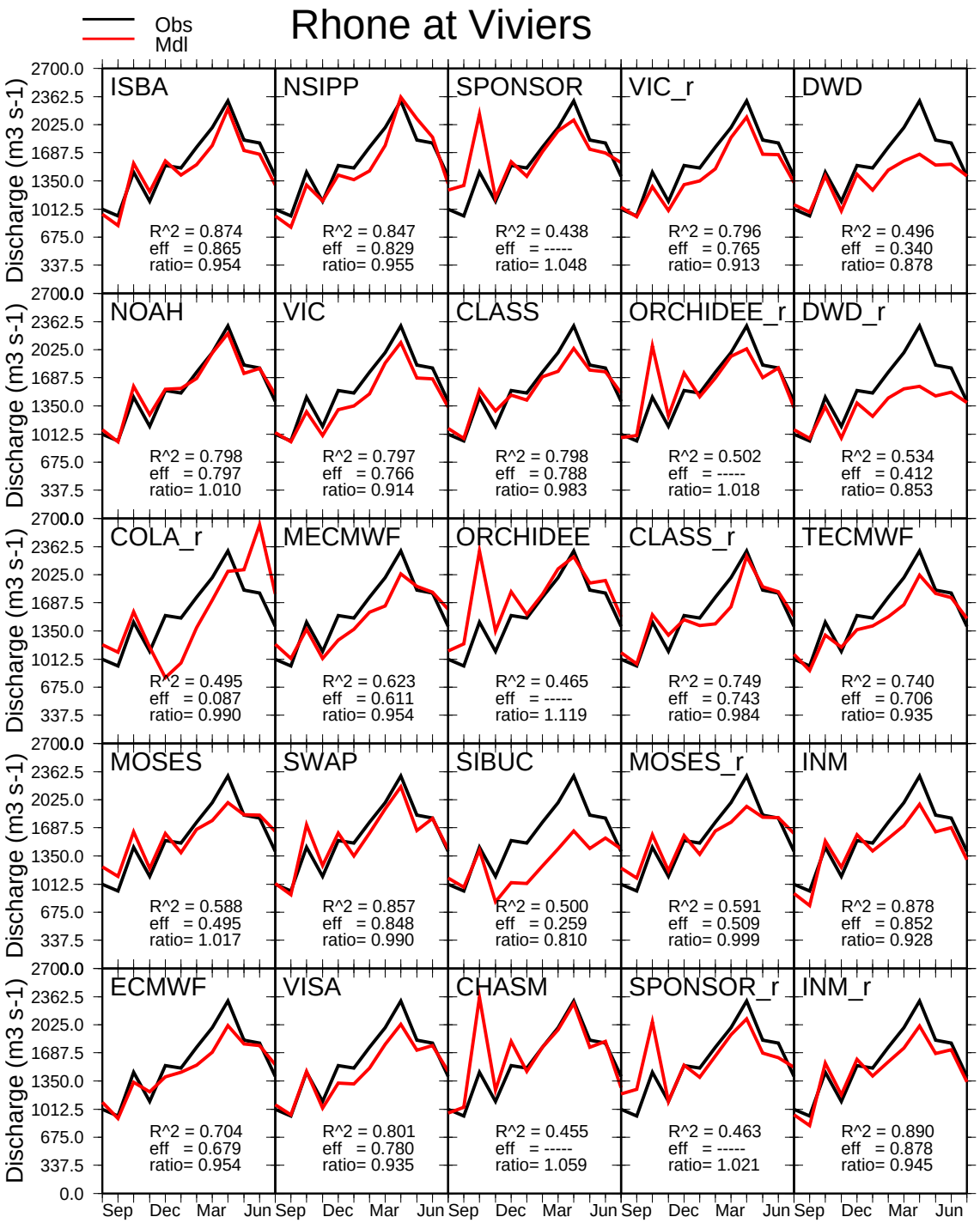

FIG. 3.13. The observed (black) and simulated (red) monthly river discharge for 25 LSS realizations for the Rhône at Viviers (see Fig. 2.1 for the location). The annual cycle averaged over 3 years is shown. The efficiency or Nash-Sutcliff coefficient (eff) (see Appendix B), squared correlation coefficient ($R\hat{2}$), and the ratio of the simulated to the observed discharges (ratio) are shown. A negative efficiency value is indicated using black lines. Statistics are computed using the daily values.

Note that all of the ELDAS LSSs capture the autumn soil recharge reasonably well: despite the peak precipitation amounts seen during this period, runoff is not excessive. However, it is important to note that several LSSs with the lowest (and similar) soil depths/soil water holding capacities (ORCHIDEE, CHASM and SPONSOR) all have excessive runoff in autumn as the soils rapidly reach their capacities. It is therefore very important to incorporate the observed soil (depth) information into the LSSs to get a reasonable runoff response.

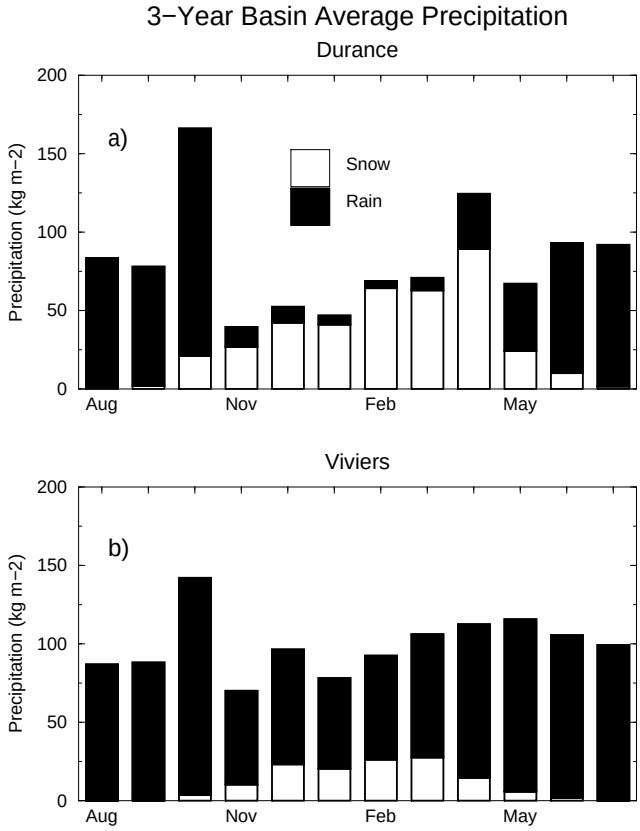

FIG. 3.14. The observed three-year average total monthly rain and snowfall for the Durance at Laclapière (panel a) and the Rhône at Viviers (panel b). The corresponding basins have surface areas of 2,170 km^2 (Durance), and over 61,000 km^2.

The LSSs have a bit more difficulty simulating the Ardeche basin (Fig. 3.15), probably owing in part to the strong influence of convection. The influence of sub-grid runoff is much more marked for this basin. The TECMWF model shows

a significant improvement over the ECMWF for this basin, primarily due to the inclusion of sub-grid runoff. The same dramatic improvement can be noted for the INM model. The DWD model tends to underestimate the winter runoff.

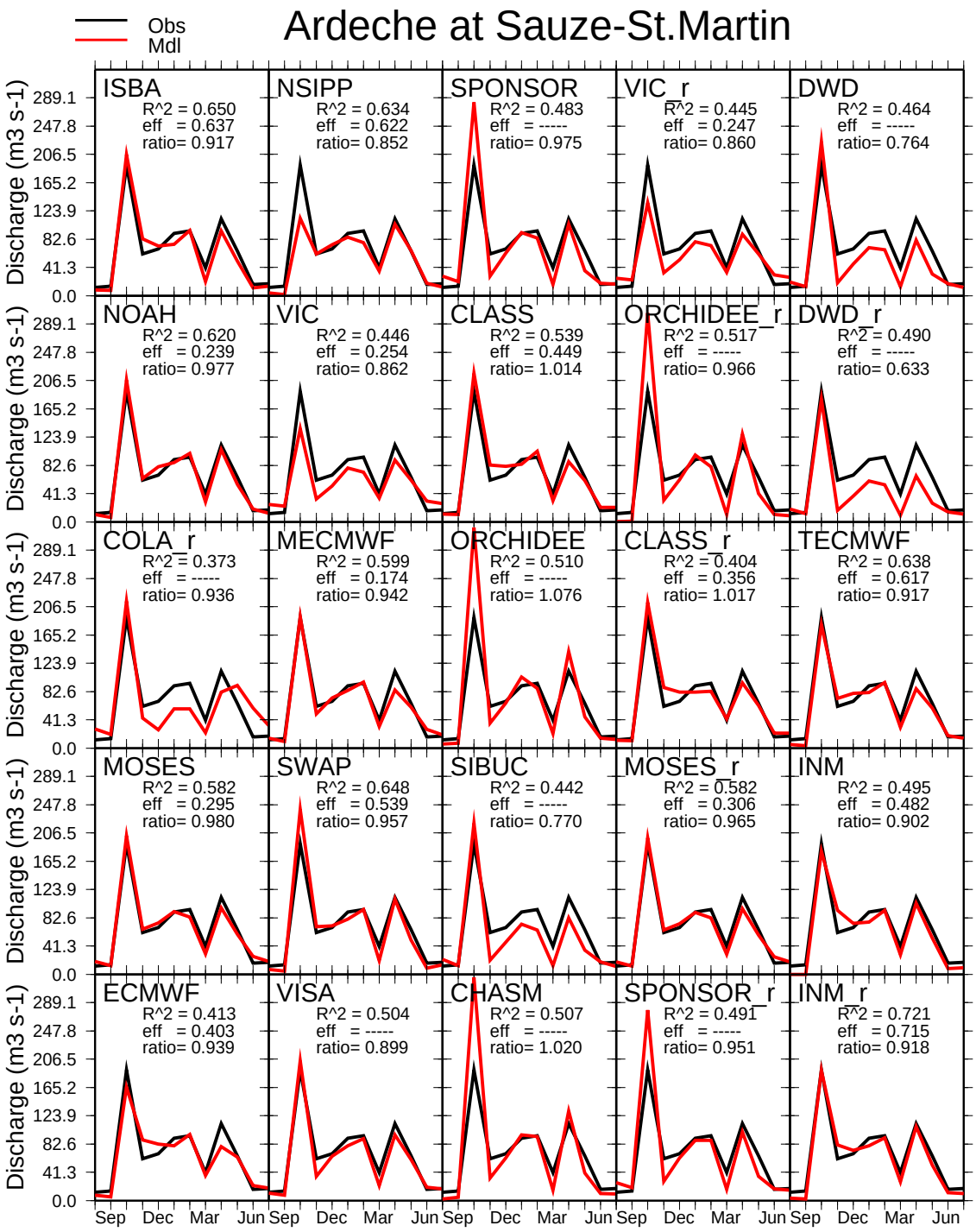

FIG. 3.15. As in Fig. 3.13, except for the Ardeche at Sauze St. Martin.

The Saone basin (Fig. 3.16) is larger than the Ardeche, and has a more frequent and stratiform precipitation regime. Sub-grid runoff is less important (as can be seen in the rather weak improvement in scores for TECMWF and INM_rerun). As was the case for Viviers, the ECMWF and DWD schemes tend to underestimate the winter runoff response.

The Durance basin (Fig. 3.17) is the most challenging of all the basins examined herein. This basin is fairly representative of a high-Alpine catchment (the average altitude is over 2000 m). A significant amount of the precipitation falls as snow (Fig. 3.14b), so that the snow model is critical for capturing the spring runoff peak (owing primarily to snowmelt). Peak winter-spring precipitation falls in April, while peak runoff is observed in June.

Only a few of the LSSs show any skill for this basin. ISBA, ECMWF and TECMWF have reasonably good snow simulations for this basin (6 of the 24 snow observation sites are included in this basin), and this is consistent with the discharge simulations. The DWD runs show a slightly early peak runoff, possibly indicating a slightly precocious snowmelt. The INM runs are very typical of those of composite snow schemes: low snow coverage results in increased evaporation (resulting in low discharge) and a significantly underestimated and early peak spring discharge.

The squared correlation coefficient as a function of surface runoff ratio (ratio of the surface runoff to the total runoff) for the Saone, Ardeche and Viviers is shown in Fig. 3.18 (the Durance is not included as snowmelt caused a very different response). The purpose of this figure is to show the impact of surface runoff ratio on the quality of the simulated discharge. Since most LSSs simulated similar total runoff, it is reasonable to compare the ratios. For all three basins, the best correlations were simulated for surface runoff ratios of about 0.20. For the largest basin (Viviers), low values also gave reasonable simulations as the effect of precipitation is more smoothed out. But for the smallest basin (Ardeche), runoff ratios between

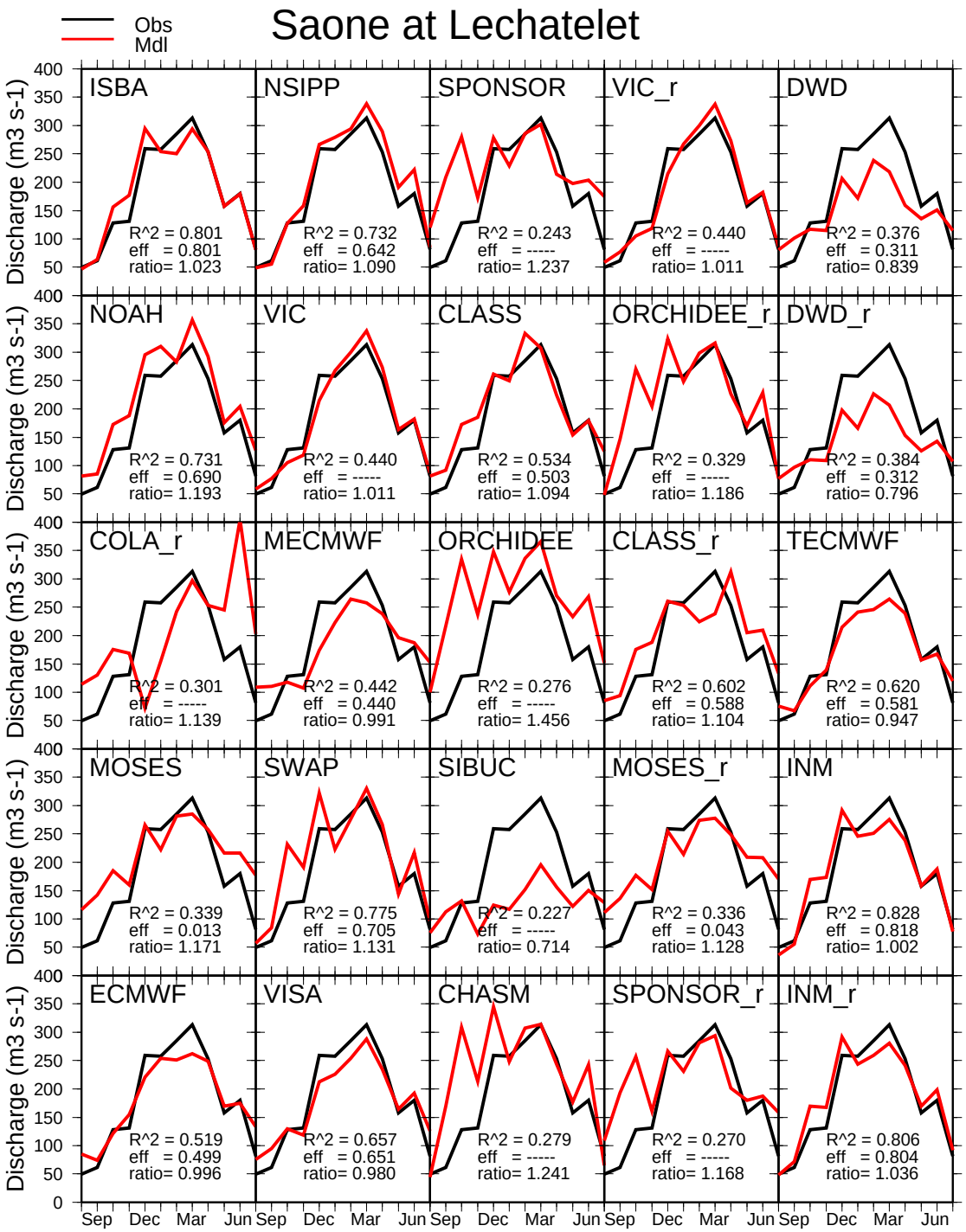

FIG. 3.16. As in Fig. 3.13, except for the Saone at Lechatelet.

approximately 0.15 and 0.25 were clearly the best. The surface runoff ratios and correlations of the ELDAS models for the Rhône at Viviers and the Ardeche at Sauze-St.Martin are shown in Table 3.3.

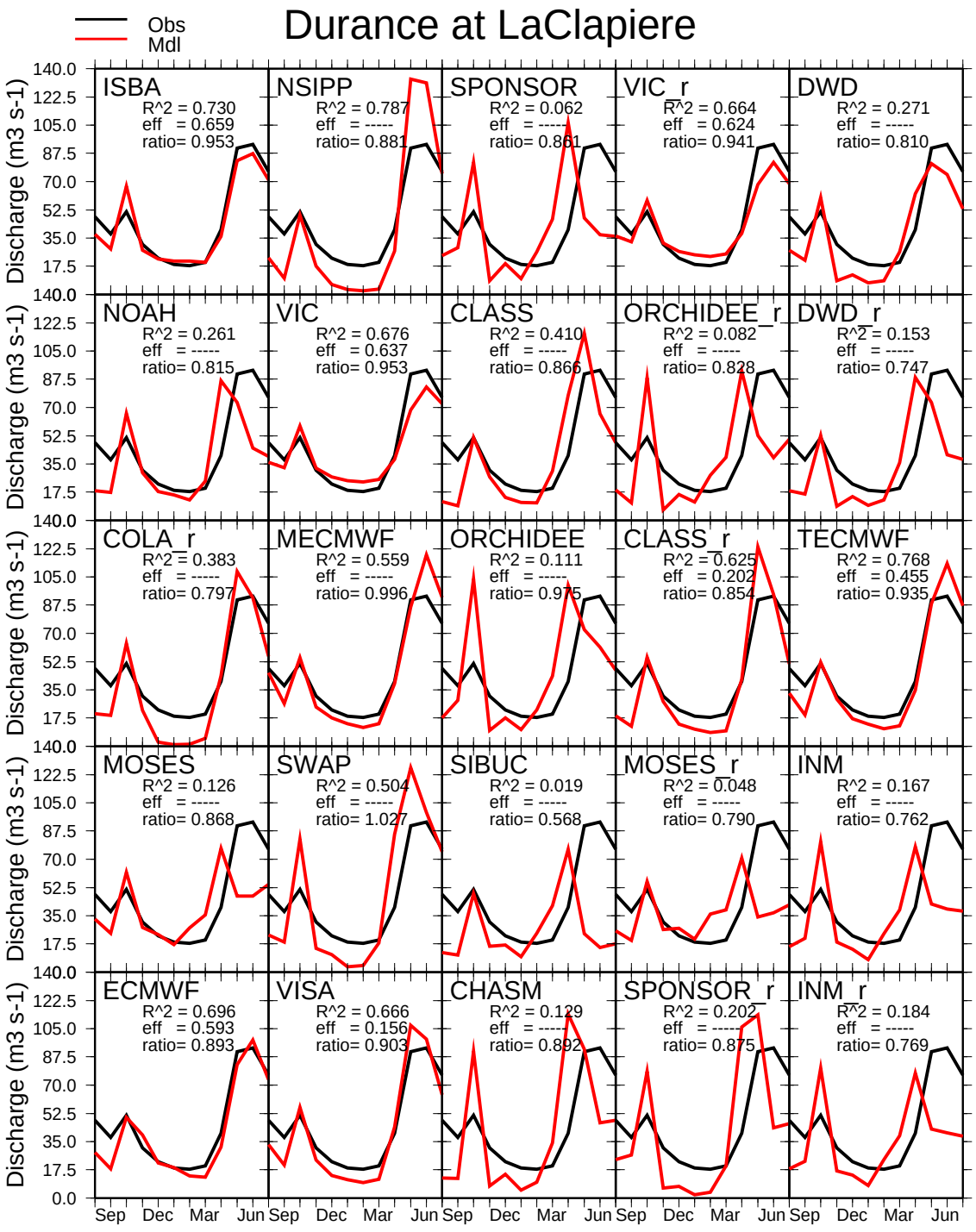

FIG. 3.17. As in Fig. 3.13, except for the Durance at la Clapière.

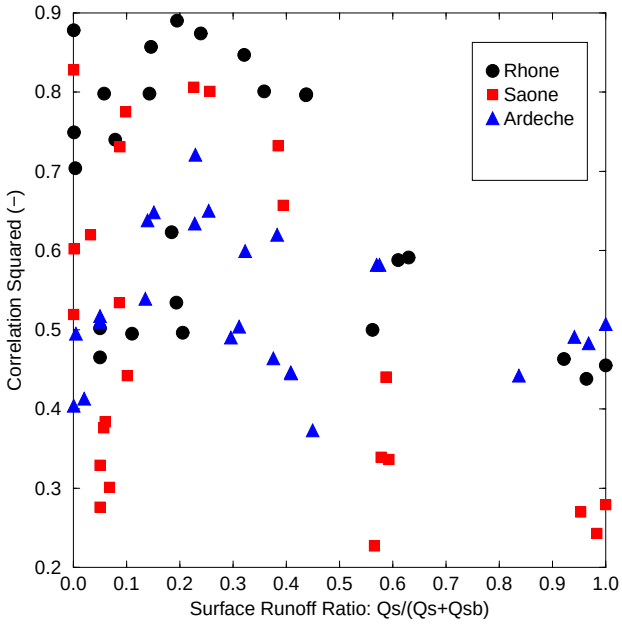

FIG. 3.18. The squared correlation coefficient as a function of surface runoff ratio (ratio of the surface runoff to the total runoff) for 3 sub-basins. Each point represents a SVAT simulation.

TABLE 3.3. The surface runoff ratios and corresponding squared correlation coefficients for the ELDAS models for the Ardeche and Rhône (at Viviers) basins. This data corresponds to points in Fig. 3.18.

LSS	Qs/(Qs+Qsb) Rhône	R^2	Qs/(Qs+Qsb) Ardeche	R^2
ISBA	0.239	0.874	0.254	0.650
ECMWF	0.003	0.704	0.020	0.413
MECMWF	0.184	0.623	0.323	0.599
TECMWF	0.078	0.740	0.139	0.638
DWD	0.205	0.496	0.375	0.464
DWD_r	0.193	0.534	0.296	0.490
INM	0.000	0.878	0.004	0.495
INM_r	0.195	0.890	0.229	0.721

2) RIVER DISCHARGE: ALL BASINS

In order to examine how the LSSs performed in terms of all of the basins, histograms of the discharge statistics were constructed. The histogram of the squared

correlation coefficient is shown in Fig. 3.19. The range is from 0 to 1, with a bin size of 1/11. The more skewed the distribution is to the right, the better the LSS performed (a perfect simulation would have all values in the rightmost bin). The effect of sub-grid runoff is more evident here. The TECMWF and INM_rerun simulations are significantly better than those of the ECMWF and INM, respectively. The ISBA and INM_rerun distributions are quite similar: and both use the same sub-grid runoff scheme and have similar soil hydrology physics and parameter values. The efficiency or Nash-Sutcliff coefficient histogram is shown in Fig. 3.20. The same general trends as for the correlation histogram can be seen.

The histogram of the ratio of the simulated to the observed discharge is shown in Fig. 3.21. Values range from 0 to 2 with a bin size of 2/11. The sharper and more centered the distribution, the better the runoff estimate by the LSS. The TECMWF histogram reveals that more basins have a ratio closer to unity compared to the ECMWF model. The DWD distribution shows a general underestimate of runoff (it is skewed to the left), which is consistent with the monthly discharge shown in Figs. 3.13,3.15, and 3.16. The INM models also tend to underestimate the runoff (they are skewed), and the distributions tend to be a bit more flat, showing more variable ratios.

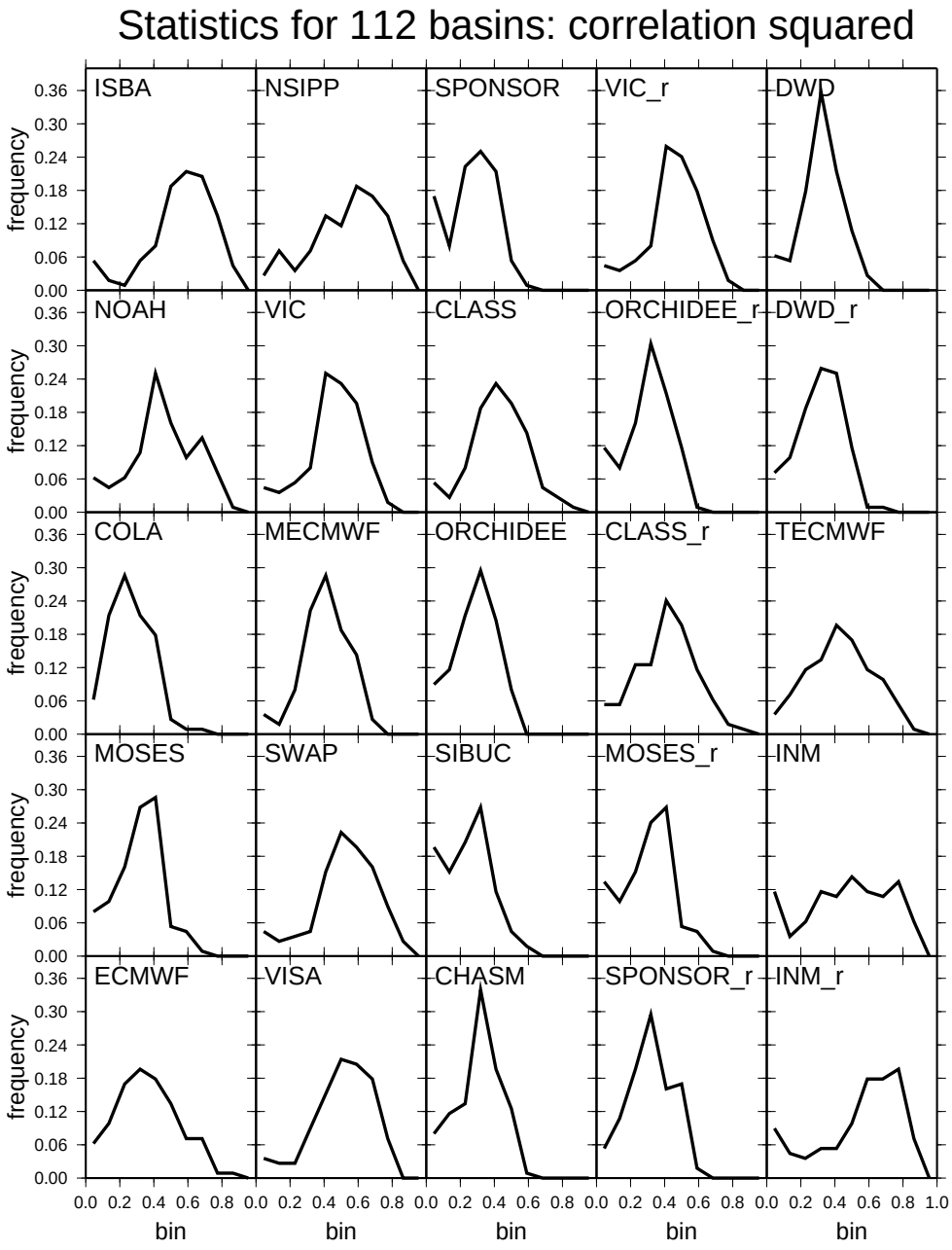

FIG. 3.19. The histogram of the normalized frequency of the correlation squared for 112 basins for each LSS realization. The range is from 0 to 1 with a bin size of 1/11. The best overall simulations are skewed the most to the right.

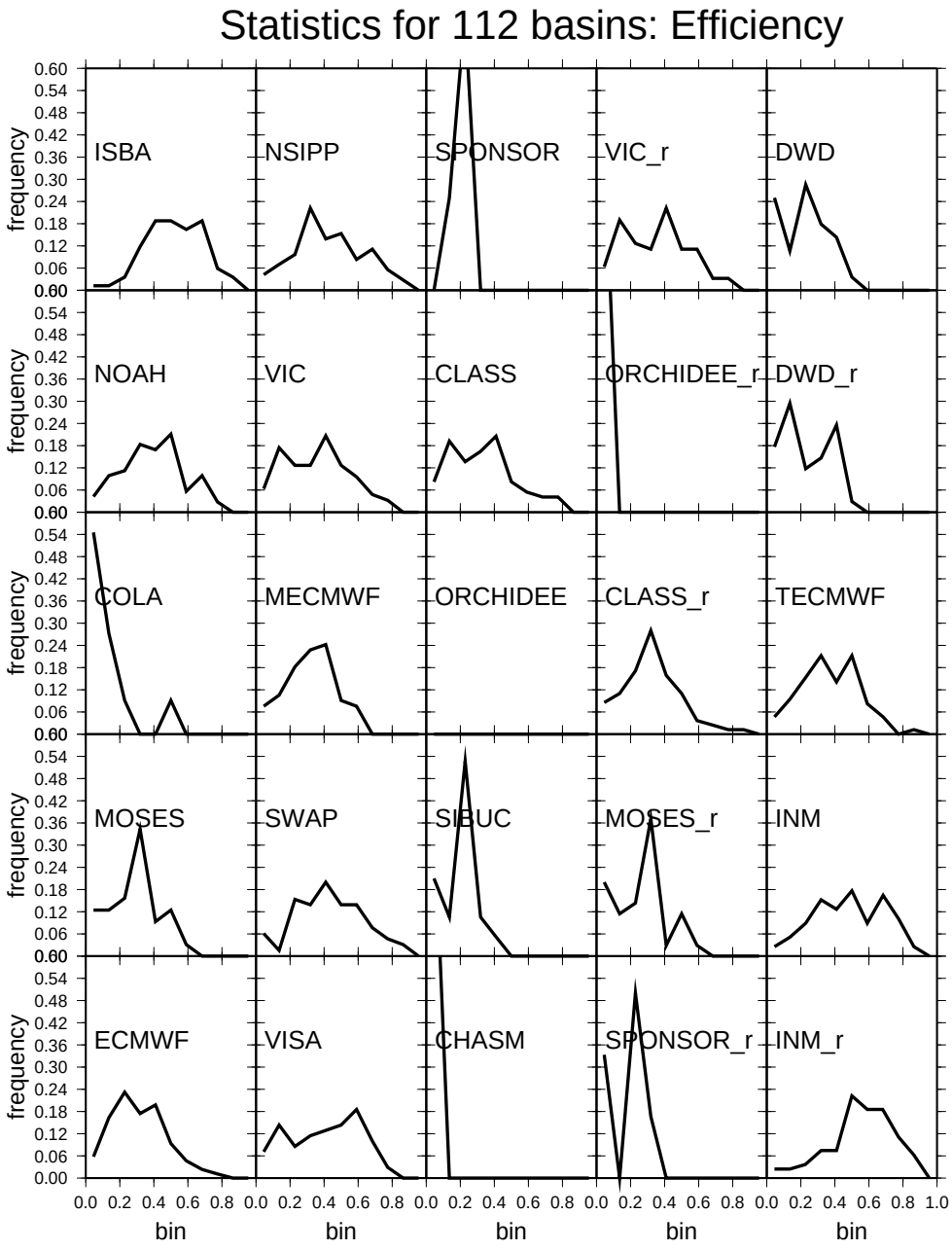

FIG. 3.20. As in Fig. 3.19, except for the efficiency. Note that negative values are not shown in the histogram, but the total number of values are used in the normalization.

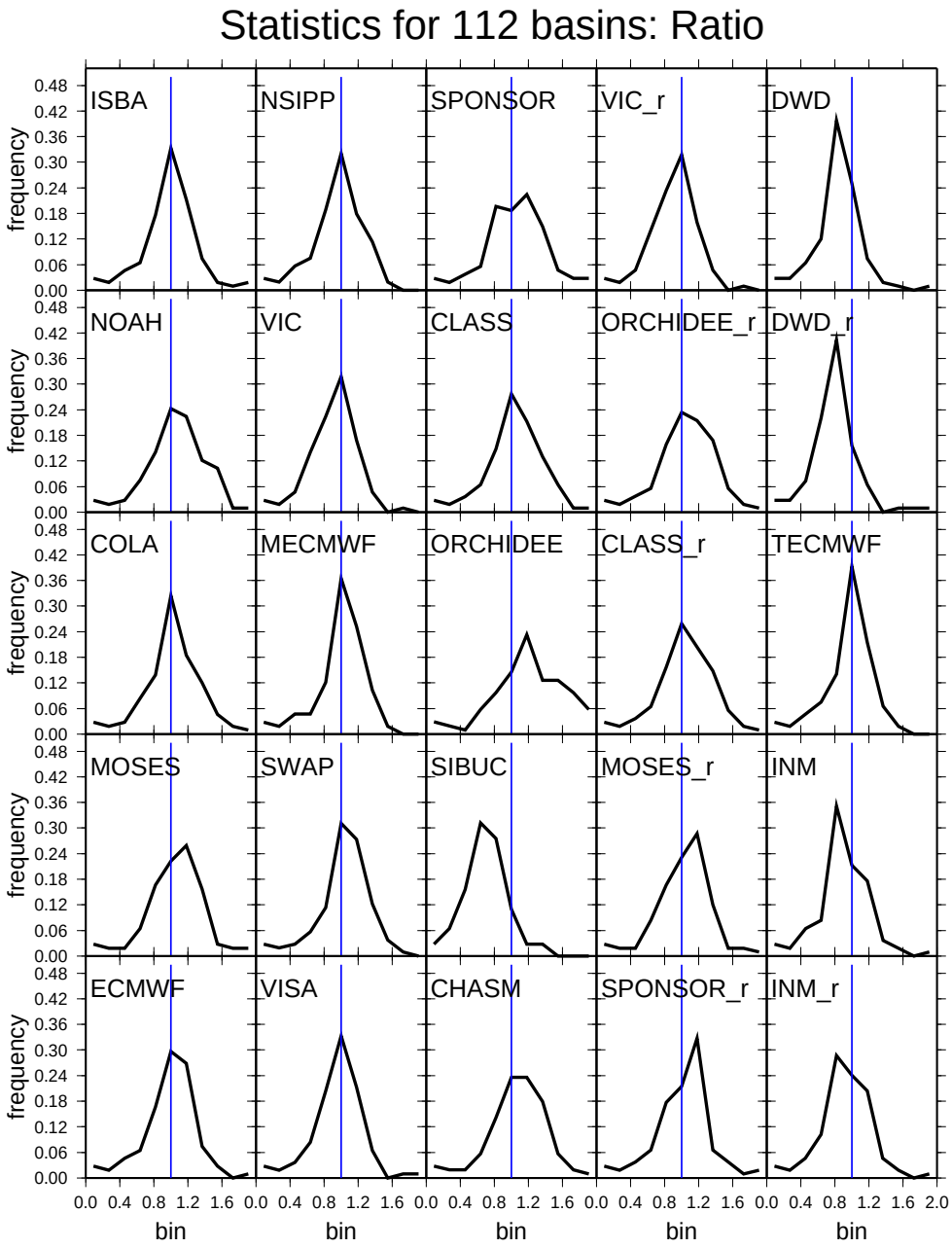

FIG. 3.21. The histogram of the normalized frequency of the ratio of the simulated to observed discharge for 112 basins for each LSS realization. The range is from 0 to 2 with a bin size of 2/11. The center of the central bin is represented by the blue line. Skewness represents a general overestimation (to right) or underestimation of runoff. The narrower and sharper the distribution (about 1), the better the simulation.

CHAPTER 4

SUMMARY

The ELDAS LSSs simulated the regional scale water and energy budgets for the Rhône basin, France, on a grid with a 8-km spatial resolution for a three year period (Aug., 1986-Jul., 1989). The Rhône-AGG control experiment (Exp1: Boone et al., 2003) setup was used: LSSs were driven in so-called "off-line" mode by atmospheric forcing, and they were given a comprehensive set of standard input soil and vegetation parameters. As a reference, the results from the Rhône-AGG LSSs are also shown (since many of these LSSs are well-known state-of-the-art models used in GCMs, NWP and hydrological modeling applications).

The ELDAS LSSs simulate the regional energy and hydrological cycles which are generally consistent with that of the Rhône-AGG LSSs. But, consistent with these LSSs, there are some important inter-scheme differences among the ELDAS models. Despite the fact that the simulated total evapotranspiration and runoff were comparable among the LSSs, the partitioning of the evapotranspiration and runoff components are significant, and lead to differences in the simulation of soil moisture and the river discharge. In addition, the snow cover simulation varied among the ELDAS schemes, with the only composite scheme greatly underestimating the snowpack (consistent with results from the Rhône-AGG).

Several of the ELDAS schemes incorporated modifications owing to results from this study. DWD significantly improved their snow simulation (DWD_rerun) compared to their baseline run. In addition, the introduction of a sub-grid runoff scheme into INM (represented by INM_rerun) and the improved soil and runoff parameters

in MECWMF (TECMWF) lead to improved discharge simulations, especially for smaller-scale basins.

Finally, the simulation of soil moisture remains problematic in the sense that most LSSs purport to simulate the actual quantity of water in the soil, yet there is virtually no agreement among the LSSs (except among very similar schemes, like ISBA and INM). Even a normalized soil water index (SWI) fails to reduce inter-model scatter. However, there is a general agreement in the time rate of change in soil moisture, at least when averaged over the entire basin. Further work is probably needed to better simulate the actual quantity of soil moisture in a more physically consistent manner among LSSs, especially in light of the current abundance of soil moisture assimilation studies. Soil moisture is to a LSS what atmospheric mixing ratio is to a NWP model, or what sea salinity is to an ocean model: it is in theory, a well-defined, measurable quantity (although with much more significant spatial heterogeneity). Further issues related to LSS soil moisture modeling will be examined as a part of Phase-2 of the GSWP (Dirmeyer et al. 1999).

APPENDIX A

ALMA VARIABLE NAMES

TABLE A.1. The ALMA (Polcher, 2001) variable name convention used within this report. See http://www.lmd.jussieu.fr/ALMA/ for details.

Variable Name	Definition	Units
ECanop	canopy interception evaporation	kg m^{-2} s^{-1}
ESoil	baresoil evaporation	kg m^{-2} s^{-1}
Evap	total evapotranspiration	kg m^{-2} s^{-1}
Qg	ground heat flux	W m^{-2}
Qh	sensible heat flux	W m^{-2}
Qle	latent heat flux	W m^{-2}
Qs	surface (overland) runoff	kg m^{-2} s^{-1}
Qsb	baseflow or drainage runoff	kg m^{-2} s^{-1}
Rnet	net radiation flux	W m^{-2}
SnowDepth	total snow depth	m
SubSnow	snow sublimation	kg m^{-2} s^{-1}
SWE	snow water (liquid) equivalent	kg m^{-2}
SWI	Soil Wetness Index	-
TVeg	transpiration	kg m^{-2} s^{-1}

APPENDIX B

STATISTICAL MEASURES

The efficiency or Nash-Sutcliff (1970) coefficient is defined as

$$\text{Eff} = 1 - \frac{\sum_{i=1}^{N} \left[Q_{sim}(i) - Q_{obs}(i)\right]^2}{\sigma_{Qobs}} \qquad (\text{Eff} \leq 1) \quad ,$$

where Q_{sim} and Q_{obs} represent the simulated and observed daily discharge, respectively. N represents the number of observation points (a maximum of one per day or 366 per year for a given site), i is the corresponding index, and σ_{Qobs} is the variance of the observed values. A value of 1 is perfect, a value of 0 means that the model is only capable of representing the average, and a negative score implies little if any relationship. The correlation coefficient is defined as the ratio of the covariance (between the observation and the simulmation) to the product of (their) variances, so that:

$$\text{R}^2 = \left\{ \frac{1}{N} \frac{\sum_{i=1}^{N} \left[Q_{obs}(i) - \overline{Q}_{obs}\right] \left[Q_{sim}(i) - \overline{Q}_{sim}\right]}{\sigma_{Qobs}\, \sigma_{Qsim}} \right\}^2 \qquad \left(0 \leq \text{R}^2 \leq 1\right) \quad .$$

REFERENCES

André, J. C., J. P. Goutorbe and A. Perrier, 1986: HAPEX-MOBILHY: A hydrologic atmospheric experiment for the study of water budget and evaporation flux at the climatic scale. *Bull. Amer. Meteor. Soc.*, **67**, 138–144.

Beljaars, A. C. M., and F. C. Bosveld, 1997: Cabauw data for the validation of land surface parameterization schemes. *J. Climate*, **10**, 1172–1193.

Boone, A., and P. Etchevers, 2001: An intercomparison of three snow schemes of varying complexity coupled to the same land-surface model: Local scale evaluation at an Alpine site. *J. Hydrometeor.*, **2**, 374–394.

Boone, A., F. Habets, J. Noilhan, D. Clark, P. Dirmeyer, S. Fox, Y. Gusev, I. Haddeland, R. Koster, D. Lohmann, S. Mahanama, K. Mitchell, O. Nasonova, G.-Y. Niu, A. Pitman, J. Polcher, A. B. Shmakin, K. Tanaka, B. van den Hurk, S. Vérant, D. Verseghy, P. Viterbo and Z.-L. Yang, 2003: The Rhone-Aggregation Land Surface Scheme Intercomparison Project: An Overview. *J. Climate*, (in press).

Bowling, L. C., D. P. Lettenmaier, B. Nijssen, L. P. Grahm, D. B. Clark, M. El Maayar, R. Essery, S. Goers, F. Habets, B. van den Hurk, J. Jin, D. Kahan, D. Lohmann, S. Mahanama, D. Mocko, O. Nasonova, A. Shmakin, D. Verseghy, P. Viterbo, Y. Xia, X. Ma, Y. Xue, and Z.-L. Yang, 2003: Simulation of high latitude hydrological processes in the Torne-Kalix basin: PILPS Phase-2(e), 1: Experiment description and summary intercomparisons. *Global and Plan. Change*, **38**, 1–30.

Champeaux, J. L., D. Acros, E. Bazile, D. Giard, J. P. Gourtorbe, F. Habets, J. Noilhan, ans J. L. Roujean, 2000: AVHRR-derived vegetation mapping over western Europe for use in numericam weather prediction models. *Int. J. Remote Sensing*, **21**, 1183–1199.

Chen, F., Z. Janic, and K. Mitchell, 1997: Impact of atmospheric surface-layer parameterizations in the new land-surface scheme of the NCEP mesoscale Eta model. *Bound.–Layer Meteor.*, **85**, 391–421.

Chen, T. H., A. Henderson-Sellers, P. C. D. Milly, A. J. Pitman, A. C. M. Beljaars, J. Polcher, F. Abramopoulos, A. Boone, S. Chang, F. Chen, Y. Dai, C. E. Desborough, R. E. Dickinson, L. Duemenil, M. Ek, J. R. Garratt, N. Gedney, Y. M. Gusev, J. Kim, R. Koster, E. Kowalczyk, K. Laval, J. Lean, D. Lettenmaier, X. Liang, J.-F. Mahfouf, H.-T. Mengelkamp, K. Mitchell, O. N. Nasonova, J. Noilhan, A. Robock, C. Rosenzweig, J. Schaake, C. A. Schlosser, J.-P. Schulz, Y. Shao, A. B. Shmakin, D. L. Verseghy, P. Wetzel, E. F. Wood, Y. Xue, Z.-L. Yang, and Q. Zeng, 1997: Cabauw experimental results from the project for intercomparison of landsurface schemes (PILPS). *J. Climate*, **10**, 1194–1215.

Clapp, R., and G. Hornberger, 1978: Empirical equations for some soil hydraulic properties, *Water Resour. Res.*, **14**, 601–604.

Desborough, C. E., 1999: Surface energy balance complexity in GCM land surface models, *Clim. Dyn.*, **15**, 389–403.

Dirmeyer, P. A., A. J. Dolman, and N. Sato, 1999: The Global Soil Wetness Project: A pilot project for global land surface modeling and validation. *Bull. Amer. Meteor. Soc.*, **80**, 851-878.

Durand, Y., E. Brun, L. Mérindol, G. Guyomarc'h, B. Lesaffre, and E. Martin, 1993: A meteorological estimation of relevant parameters for snow schemes used with atmospheric models. *Ann. Glaciol.*, **18**, 65–71.

Entin, J. K., A. Robock, K. Y. Vinnikov, V. Zabelin, S. Liu, A. Namkhai, and Ts. Adyasuren, 1999: Evaluation of Global Soil Wetness Project soil moisture simulations. *J. Meteor. Soc. Japan*, **77**, 183–198.

Essery, R. L. H., Best, M. J., Betts, R. A., Cox, P. M., Taylor, C. M.. 2003: Explicit Representation of Subgrid Heterogeneity in a GCM Land Surface Scheme. *J. Hydrometeor.*, **4**, 530–543.

Etchevers, P., C. Golaz and F. Habets, 2001: Simulation of the water budget and the river flows of the Rhône basin from 1981 to 1994. *J. Hydrol.*, **244**, 60–85.

Giordano, A., and Coauthors, 1990: CORINE soil erosion risk and important land resources. *Tech. Rep. 13233 EN, EUR*, Eur. Communities.

Golaz-Cavazzi, C., P. Etchevers, F. Habets, E. Ledoux and J. Noilhan, 2001: Comparison of two hydrological simulations of the Rhone basin, *Phys. and Chem. of the Earth*, Part B: Hydrology, Oceans and Atmosphere, **26**, 461–466.

Gusev, Ye. M., and O. N. Nasonova, 1998: The land surface parameterization scheme SWAP: description and partial validation. *Global and Plan. Change*, **19**, 63–86.

Habets, F., J. Noilhan, C. Golaz, J.P. Goutorbe, P. Lacarrère, E. Leblois, E. Ledoux, E. Martin, C. Ottlé, and D. Vidal-Madjar, 1999a: The ISBA surface scheme in a macroscale hydrological model applied to the HAPEX-MOBILHY area Part 1: Model and database. *J. Hydrol.*, **217**, 75–96.

Habets, F., R. Etchevers, C. Golaz, E. Leblois, E. Ledoux, E. Martin, J. Noilhan, and C. Ottlé, 1999b: Simulation of the water budget and the river flows of the Rhone basin. *J. of Geophys. Res.*, **104**, 31145–31172.

Henderson–Sellers, A., Z.–L. Yang and R. E. Dickinson, 1993: The project for intercomparison of land–surface parameterization schemes. *Bull. Amer. Meteor. Soc.*, **74**, 1335–1349.

Henderson–Sellers, A., A. Pitman, P. Love, P. Irannejad, and T. Chen, 1995: the project of intercomparison of land-surface parameterization schemes (PILPS): Phases 2 and 3. *Bull. Amer. Meteor. Soc.*, **94**, 489–503.

King, D., C. Lebas, M. Jamagne, R. Hardy, and J. Draoussin, 1995: Base de données géographiques des sols de France à l'échelle 1/1000000 (Geographical Soil Database for France at a scale of 1/1000000). *Technical Report*, Institut National de Recherches Agronomiques (INRA), Orleans, France, 100 pp.

Koster, R. D., and P. C. D. Milly, 1997: The interplay between transpiration and runoff formulations in land surface schemes used with atmospheric models. *J. Climate*, **10**, 1578–1591.

Koster, R.D., M.J. Suarez, A. Ducharne, M. Stieglitz, and P. Kumar, 2000: A catchment-based approach to modeling land surface processes in a general circulation model: 1. Model structure. *J. of Geophys. Res.*, **105**, 24,809–24,822.

Ledoux, E., G. Girard, G. de Marsilly, J. Deschenes, 1989: Spatially distributed modeling: conceptual approach, coupling surface water and ground water, NATO, ASI Series C. In: Morel-Seytoux, X. (Ed.). Unsaturated Flow Hydrologic Modeling-theory and Practice, 275 pp. Kluwer Academic, Dordrecht pp. 435–454.

Liang, X., D. Lettenmaier, E. F. Wood, and S. J. Burges, 1994: A simple hydrologically based model of land surface water and energy fluxes for general circulation models, *J. of Geophys. Res.*, **99**, 14,415–14,428.

Meeson, B. W., F. E. Corprew, J. M. P. McManus, D. M. Meyers, J. W. Closs, K.-J. Sun, D. J. Sunday, and P. J. Sellers, 1995: ISLSCP Initiative I-Global Data Sets for Land-Atmosphere Models, 1987-1988. Volumes 1-5. Published on CD by NASA (USA_NASA _GDAAC _ISLSCP_001 - USA_NASA _GDAAC _ISLSCP_005).

Nash, J. E., and J. V. Sutcliffe, 1970: River flow forecasting through conceptual models. Part I: A discussion of principles. *J. Hydrol.*, **10**, 282–290.

Noilhan, J. and J.-F. Mahfouf, 1996: The ISBA land surface parameterization scheme. *Global and Plan. Change*, **13**, 145–159.

Polcher, J., 2001: GLASS Implementation underway. *GEWEX News*, WCRP, **10**, 9.

Rodríguez, E., B.Navascués, J.J. Ayuso, and S. Jarvenoja, 2003: Analysis of surface variables and parameterization of surface processes in HIRLAM, Part I: Approach and verification by parallel runs. HIRLAM Technical Report No. 58, January.

de Rosnay, P., and J. Polcher, 1998: Modeling root water uptake in a complex land surface scheme coupled to a GCM, *Hydrology and Earth System Sciences*, **2**, 239–356.

Schlosser, C. A., A. G. Slater, A. Robock, A. J. Pitman, K. Y. Vinnkov, A. Henderson-Sellers, N. A. Speranskaya, K. Mitchell, A. Boone, H. Braden, F. Chen, P. Cox, P. de Rosnay, C. E. Desborough, R. E. Dickinson, Y.-J. Dai, Q. Duan, J. Entin, P. Etchevers, N. Gedney, Y. M. Gusev, F. Habets, J. Kim, V. Koren, E. Kowalczyk, O. N. Nasonova, J. Noilhan, J. Schaake, A. B. Shmakin, T. G. Smirnova, D. Verseghy, P. Wetzel, Y. Xue, and Z.-L. Yang, 2000: Simulations of a boreal grassland hydrology at Valdai, Russia: PILPS Phase 2(d). *Mon. Wea. Rev.*, **128**, 301–321.

Schrodin, R., and E. Heise, 2001: The multi-layer version of the DWD soil model TERRA-LM. COSMO Technical Report **2**, Sept. 2001, 17 pp.

Sellers, P. J. and Coauthors, 1997: BOREAS in 1997: Experiment overview, scientific results, and future directions. *J. of Geophys. Res.*, **102**, 28731–28769.

Sellers, P. J., B. W. Meeson, J. Closs, J. Collatz, F. Corprew, D. Dazlich, F. G. Hall, Y. Kerr, R. Koster, S. Los, K. Mitchell, J. McManus, D. Meyers, K.-J. Sun, and P. Try, 1995: An overview of the ISLSCP Initiative I Global Data

Sets for Land-Atmosphere models, 1987-1988. Volumes 1-5. Published on CD by NASA. Volume 1: USA_NASA_GDAAC_ISLSCP_001, OVERVIEW.DOC.

Sellers, P. J., F. G. Hall, G. Asrar, D. E. Strebel, R. E. Murphy, 1988: The first ISLSCP Field Experiment (FIFE), *Bull. Amer. Meteor. Soc.*, **69**, 22–27.

Shao, Y. and A. Henderson-Sellers, 1996: Validation of soil moisture simulation in land surface parameterization schemes with HAPEX data. *Global and Plan. Change*, **13**, 11–46.

Shmakin, A.B., 1998: The updated version of SPONSOR land surface scheme: PILPS-influenced improvements. *Global and Plan. Change*, **19**, 49–62.

Slater, A. G., C. A. Schlosser, C. E. Desborough, A. J. Pitman, A. Henderson-Sellers, A. Robock, K. Ya. Vinnikov, K. Mitchell, A. Boone, H. Braden, F. Chen, P. M. Cox, P. de Rosnay, R. E. Dickinson, Y.-J. Dai, Q. Duan, J. Entin, P. Etchevers, N. Gedney, Ye. M. Gusev, F. Habets, J. Kim, V. Koren, E. A. Kowalczyk, O. N. Nasonova, J. Noilhan, S. Schaake, A. B. Shmakin, T. G. Smirnova, D. Verseghy, P. Wetzel, Y. Xue, Z.-L. Yang, Q. Zeng, 2001: The Representation of Snow in Land Surface Schemes: Results from PILPS 2(d). *J. Hydrometeor.*, **2**, 7–25.

Tanaka, K., E. Nakakita, ans S. Ikebuchi, 1998: Land-surface parameterization in the Lake Biwa Project. *Annual Journal of Hydraulic Engineering*, Japan Society of Civil Engineers, **42**, 79–84.

Van den Hurk, B., P. Viterbo, A. C. M. Beljaars and A. K. Betts, 2000, Offline validation of the ERA40 surface scheme; ECMWF Technical Memo 295.

Van den Hurk, B., and P. Viterbo, 2002: The Torne-Kalix PILPS-2e experiment as a test bed for modifications to the ECMWF land surface scheme. *Global and Plan. Change*, **38**, 165–173.

Van Genuchten, M. T., 1980: A closed form equation for predicting the hydraulic conductivity of unsaturated soils. *Soil Sci. Soc. Am.*, **44**, 892–898.

Verseghy, D., 2000: The Canadian LAnd Surface Scheme (CLASS): Its history and future. *Atmosphere-Ocean*, **38**, Special Issue on CLASS, 1–3.

Violette, S., E. Ledoux, P. Goblet, and J. P. Carbonnel, 1997: Hydrologic and thermal modeling of an active volcano: the Piton de la Fournaise, Reunion. *J. Hydrol.*, **191**, 37–63.

Wood, E. F., D. Lettenmaier, X. Liang, D. Lohmann, A. Boone, S. Chang, F. Chen, Y. Dai, C. Desborough, Q. Duan, M. Ek, Y. Gusev, F. Habets, P. Irannejad, R. Koster, O. Nasanova, J. Noilhan, J. Schaake, A. Schlosser, Y. Shao, A. Shmakin, D. Verseghy, J. Wang, K. Warrach, P. Wetzel, Y. Xue, Z.-L. Yang and Q. Zeng, 1998: The Project for Intercomparison of Land-Surface Parameterization Schemes (PILPS) Phase-2c Red-Arkansas River Basin experiment: 3. experiment description and summary intercomparisons. *Global and Plan. Change*, **19**, 115–135.

Xue, Y., P.J. Sellers, J.L. Kinter and J. Shukla, 1991: A simplified biosphere model for global climate studies. *J. Climate*, **4**, 345–364.

Yang, Z.-L., and G.-Y. Niu, 2002: The versatile integrator of surface and atmospheric processes (VISA) Part 1: Model description. *Global and Plan. Change*, (in press).